Most bivalves and gastropods calcify indistinguishably from dual clumped isotope equilibrium

Vanessa Schlidt[1*], David Evans[1,2], Niels J. de Winter[3], Miguel Bernecker[1], Iris Arndt[1], Philip T. Staudigel[1], Amelia J. Davies[1,4], Uwe Brand[5], Wolfgang Müller[1], Jens Fiebig[1*]

[1]Institute of Geosciences, Goethe University Frankfurt, Altenhöferallee 1, 60438 Frankfurt am Main, Germany
[2]Now at: School of Ocean and Earth Science, University of Southampton, Southampton, UK
[3]Department of Earth Sciences, Vrije Universiteit Amsterdam, the Netherlands
[4]Now at: Institute for Geology and Mineralogy, University of Cologne, Cologne, Germany
[5]Department of Earth Sciences, Brock University, St. Catharines, Ontario, Canada

*corresponding authors: e-mail: schlidt@em.uni-frankfurt.de; Jens.Fiebig@em.uni-frankfurt.de

Abstract

Molluscan shell-carbonates are extensively used to reconstruct paleo-temperatures at sub-annual resolution. The accurate application of two widely used temperature proxies, the shell carbonate oxygen isotope ($\delta^{18}O$) and carbonate clumped isotope (Δ_{47}) composition, is based on the assumption that kinetic processes in the DIC-H_2O-$CaCO_3$ system were either absent or invariant during shell formation, and thus can be corrected for using empirical calibrations. Here, we analysed the dual clumped isotope composition, Δ_{47} and Δ_{48}, of a wide range of modern and Eocene molluscs (bivalves and gastropods) to investigate the potential importance of kinetics during molluscan biomineralisation. We show that Δ_{47} and Δ_{48} values of most of our modern samples are indistinguishable from equilibrium. For these samples, Δ_{47}-derived temperatures conform to corresponding growth temperatures within their fully propagated 95% uncertainties of ≤ +/-2.3°C. Significant departures from equilibrium values were only observed for a single gastropod specimen characterised by a growth temperature <10°C. Together, these results strongly imply that bivalve and gastropod shell carbonate archives can be used for accurate and highly precise reconstructions of sea surface temperatures by means of clumped

Commented [DE1]: Kinetics was (but it sounds wrong), or Processes were

isotope thermometry. Kinetic biases on this thermometer, if relevant at all, may only become important at relatively low temperatures.

Δ_{47}-derived temperatures for our Eocene samples (~39 Ma) from the Hampshire Basin (paleo-latitude ~40°N) range from 17.3 to 23.2°C. These paleo-temperatures are in agreement with sea surface temperatures for mid-Eocene mid latitude regions based on foraminifera clumped isotopes; adding confidence to both datasets. In order to aid the accurate reconstruction of seawater $\delta^{18}O$ values, we compiled published oxygen isotope fractionation data for molluscs and established relationships that describe the temperature dependence of oxygen isotope fractionation between water and molluscan calcite and aragonite, respectively.

Comment: can we insert the equation(s) here??

Applying the equation for aragonite to the Eocene samples, we obtain reconstructed seawater $\delta^{18}O$ values for the Hampshire Basin between -2.3 and -3.5‰ (VSMOW), similarly in agreement with previous approaches suggesting a freshwater-influenced surface ocean composition in this region.

Commented [DE2]: Otherwise you simply end on a number with no explanation of its significance

Keywords

Carbonate clumped isotopes, molluscs, biomineralisation, paleoclimate

1. Introduction

Accurate reconstruction of Earth's surface temperatures during periods of elevated atmospheric CO_2 levels is of great importance for testing the skill of climate models that are used to predict future climate change. To accomplish this task, it is necessary to identify geochemical proxies and sedimentary archives that reliably record Earth's surface temperatures in deep time. This is important, because the most recent time interval characterised by a global climate state similar

to the worst-case end-of-century CO_2 predictions occurred millions of years ago (e.g., Judd et al., 2024).

Molluscan shells represent an archive that potentially enables accurate climate reconstruction across such an extent of geological time. Molluscs make up one of the most diverse groups of calcifying organisms on Earth, inhabiting a wide range of terrestrial and marine habitats. Their (continuous) occurrence in the fossil record reaches back as far as the early Cambrian (e.g., Immenhauser et al., 2016 and references therein), and they achieved dominance in abundance over brachiopods by the end of the Permian (Payne et al., 2014). Molluscs form shells of calcite, aragonite, and sometimes high-Mg calcite and vaterite (Nehrke et al., 2012), or combinations thereof. Mollusc-based paleo-temperature reconstructions have predominantly utilised the oxygen isotope composition ($\delta^{18}O$) of their shells (e.g., Schöne et al., 2005; Butler et al., 2015; Huyghe et al., 2015; de Winter et al., 2020, Ivany et al., 2022; Arndt et al., 2024), requiring the oxygen isotope composition of seawater to be known or assumed.

The carbonate clumped isotope thermometer (Ghosh et al., 2006) avoids this issue as it is based on the temperature dependence of the Δ_{47} value. This value compares the abundance of ^{13}C-^{18}O-bearing isotopologues in the CO_2 derived from phosphoric acid digestion of carbonates with its stochastically predicted abundance (Ghosh et al., 2006), which is independent of the oxygen isotope composition of seawater. Nonetheless, the attainment of homogeneous isotopic equilibrium in the solution from which $CaCO_3$ is precipitated (i.e., the isotopic equilibration between water and the DIC species) is a requirement for accurate temperature reconstructions using the Δ_{47}-thermometer in the absence of empirical calibration. However, recent studies have revealed that many biogenic carbonates (e.g., corals, brachiopods, echinoids, and cephalopods) or inorganic carbonates (e.g., speleothems) record Δ_{47} signatures that are affected by kinetics (Affek, et al., 2014; Affek & Zaarur, 2014; Bajnai et al., 2018, 2020; Daeron et al., 2011; Davies & John, 2019; Davies et al., 2021; Guo, 2020; Guo & Zhou, 2019; Saenger et al., 2012, 2017).

The rate-limiting process in the equilibration of both clumped and oxygen isotopes within the DIC-H_2O-$CaCO_3$ system is the interconversion of aqueous CO_2 and HCO_3^- via (de)hydration and (de)hydroxylation reactions. If the precipitation rate of carbonate outpaces the equilibration rate of the DIC pool, the disequilibrium isotopic signatures present in the DIC pool will be inherited by the forming. The direction and magnitude of these kinetic biases is governed by processes such as addition or removal of CO_2, that can perturb the state of DIC during mineral formation (Guo, 2020). Since both the oxygen and clumped isotope composition of a carbonate follow the same chemical exchange reactions, $\delta^{18}O_{carb}$ and Δ_{47} can be used in conjunction to detect potential kinetic biases (e.g., Bajnai et al., 2018). However, there are two potential problems with this technique: 1) uncertainties introduced by the absence of knowledge of paleo-water $\delta^{18}O$ values impairs the application of paired $\delta^{18}O_{carb}$ and Δ_{47} measurements in diagnosing kinetic biases in fossil archives, and 2) the presence of kinetic bias in carbonate formation temperatures derived from oxygen isotope and Δ_{47} thermometry, although this may be overcome by applying species-specific temperature calibrations (e.g., Weber & Woodhead, 1972; McConnaughey et al., 1989a; Davies et al., 2023) provided disequilibrium offsets are invariant through space and time.

The addition of a second thermodynamically controlled metric that is independent of fluid-$\delta^{18}O$ has become possible through high-precision Δ_{48} analysis, which addresses measured and stochastic abundances of m/z 48 isotopologues (mainly $^{12}C^{18}O_2$) in the CO_2 evolved from phosphoric acid digestion of carbonates (Fiebig et al., 2019). Changes in Δ_{47} and Δ_{48} values and their precursors, Δ_{63} and Δ_{64}, respectively in the carbonate are controlled by the same chemical processes. The simultaneous measurement of both Δ_{47} and Δ_{48} by dual clumped isotope analysis, allows isotopic disequilibrium signatures to be identified and the extent of disequilibrium to be assessed. It also enables identification of the underlying process through which carbonate precipitation was initiated by comparing measured dual clumped isotope data with the position of Δ_{47}-Δ_{48}-equilibrium (e.g., Bajnai et al., 2020; Fiebig et al., 2021). For

Commented [PS3]: There are many citations that would support this statement.

Commented [DE4]: I rephrased slightly as otherwise it isn't clear how the last sentence of this paragraph relates to that before it.

Commented [DE5]: I prefer the original here

example, if supersaturation and precipitation is concurrent with CO_2 absorption, as is the case in corals (e.g., Thiagarajan et al., 2011; Saenger et al., 2012; Spooner et al., 2016) kinetic limitation will be expressed in positive Δ_{47} and negative Δ_{48} offsets from equilibrium (Guo, 2020; Bajnai et al., 2020). If, on the contrary, supersaturation and precipitation is accompanied with or driven by net CO_2 degassing, as is characteristic for speleothems, kinetic limitation evokes $-\Delta_{47}/+\Delta_{48}$ disequilibrium patterns (Guo & Zhou, 2019; Guo, 2020; Bajnai et al., 2020). Since its invention, dual clumped isotope thermometry has been used to identify kinetic bias in cold and warm water corals (Davies et al., 2022), brachiopods (Davies et al., 2023), bird eggshells (Tagliavento et al., 2023), speleothems (Bajnai et al., 2020, Parvez et al., 2024), authigenic methane seep carbonates (Staudigel et al., 2024), freshwater cements (Lu et al., 2024), microbial carbonates (Ingalls et al., 2024; Lu & Swart, 2024), and in carbonates associated with the serpentinisation of ultramafic rocks (Parvez et al., 2023). Crucially, it has been shown that kinetic biases in corals, brachiopods, speleothems and methane seep carbonates follow identifiable model-predicted disequilibrium trajectories. These can be used to correct measured dual clumped isotope data and, finally, to isolate the temperature signal recorded in the carbonate. If, on the contrary, kinetic biases remain undetected, and no empirical calibration is available for an archive of interest, these would result in erroneous growth temperature reconstructions from measured Δ_{47} values. Such reconstructed growth temperatures would be over-estimated or underestimated if CO_2 removal or CO_2 absorption, respectively, were rate-limiting.

Previous investigations revealed that kinetic biases in Δ_{47} values of mollusc shells, if present at all, might only be weakly pronounced. Huyghe et al. (2022) and de Winter et al. (2022) analysed shells of marine bivalves and oysters grown at temperatures of -2 to 27°C. With the exception of juvenile oysters, Δ_{47} values obtained by Huyghe et al. (2022) agreed with those predicted by the unified calibration of Anderson et al. (2021) which, in turn, is indistinguishable from the inorganic calcite equilibrium Δ_{47}-T relationship of Fiebig et al. (2021). On the contrary,

Commented [DE6]: Why don't we measure the earlier work of Petrizzo et al. (2014) here? I appreciate things have moved on a lot, but the overall finding is similar.

formation temperatures for *A. islandica* were slightly, but significantly (2.7 ± 2.0°C) underestimated by de Winter et al. (2022) who also projected Δ_{47} values to the Anderson et al. (2021) relationship. Curley et al. (2023) investigated fossil bivalves of unconstrained growth temperatures. Based on intra-shell alignments between Δ_{47} and $\delta^{18}O_{carb}$ they postulated that the inner shell layer is prone to kinetic isotope effects, whereas the outer shell layer is not.

In this study, we analysed the dual clumped isotope composition of twelve modern and five fossil mollusc species for a total of 21 specimens to investigate whether their clumped isotope composition is affected by rate-limiting kinetics. We demonstrate that our sampled shells calcify indistinguishably from dual clumped isotope equilibrium which would make bivalves and gastropods excellent archives for high-precision paleo-temperature reconstructions of moderate to warm climates. We also compile mollusc-specific aragonite and calcite oxygen isotope data in order to refine the $1000\ln\alpha(CaCO_3\text{-}H_2O)$-T relationships for both molluscan aragonite and calcite. Finally, we apply the dual clumped isotope thermometer to five Eocene molluscs from the Hampshire Basin, reconstruct sea surface temperatures and seawater-^{18}O, and compare these estimates to results previously reconstructed for the same geographic region and age.

Commented [DE7]: This addition to the sentence only makes sense if we keep the part about disequilibrium at low T, otherwise why do we specify moderate/warm?

Commented [DE8]: We do demonstrate equilibrium in most cases and we do compile d18O data - no need for hope to/aim to.

Commented [DE9]: Some explanation of the aim is helpful here, I think, so I added this.

2. Material and Methods

We analysed twenty-one molluscan samples for their dual clumped and bulk stable isotope compositions, consisting of sixteen modern and five specimens from the mid Eocene (Bartonian; ~39 Myr). Metadata for all samples are in Table 1.

2.1 Modern samples

Names and details of modern specimens measured in this study are provided in Table 1. Independently constrained growth temperatures and independently constrained $\delta^{18}O_{SW}$ values of these samples are listed in Table 2.

157 The bivalves *Modiolus modiolus* (RM1) and *Spisula solida* (RM2) as well as the gastropods
158 *Buccinum undatum* (RG1) and *Patella vulgata* (RG2) were collected at low tide from a beach
159 in southeast Scotland (Tentsmuir Forest) in March 2020. The average annual sea surface
160 temperature for the site of sample collection is 9.6°C determined using the World Ocean Atlas
161 (WOA) 2023 (Locarnini et al., 2024), with a seasonal range of 7.0-12.4°C. The oxygen isotope
162 composition of seawater at the site of sample collection ($\delta^{18}O_{sw}$) was 0.2‰ (VSMOW),
163 calculated based on gridded data provided by Harwood et al. (2008).
164 Some material for this study came from a population of cultured bivalves: *Arctica islandica*
165 (AL_006) and *Mytilus edulis* (ME_002, ME_003) cultured at NIOZ (Royal Netherlands
166 Institute for Sea Research). Growth temperatures for bivalves ME_002 and ME_003 range
167 between 5 and 25°C (seasonal temperature changes were imposed) with an average temperature
168 of 16.2°C during the culturing period. Bivalve AL_006 was cultured at a constant temperature
169 of 12.0°C.
170 M2-Sf and M2-Sv are sample powders from a cultured *Magellana gigas* (cf. *Crassostreas*
171 *gigas*) specimen (additional geochemical data published in de Winter et al., 2021a). The
172 imposed seasonal range of temperature for bivalves M2-Sf and M2-Sv varies between 4
173 and19°C with a mean of 11.5°C. Reconstructed $\delta^{18}O_{sw}$ value (VSMOW) is -1.55 ‰ (de Winter
174 et al., 2021a). CHA_M_050 and CHA_M_062 are *A. islandica* specimens collected off the
175 coast of NE Iceland (Pederson et al., 2019). The WOA2023-derived annual mean growth
176 temperature is 3.9°C (Locarnini et al., 2024), while summer temperatures reach 7.4°C. Dual
177 clumped isotope data on these two samples has already been reported but discussed in a
178 different context by Staudigel et al. (2023a). Bivalve shells UC and UH are *Hippopus*
179 *porcellanus* specimens purchased at an antique trade; growth temperature and $\delta^{18}O$ values of
180 the water are therefore unknown although their growth temperatures can be estimated given
181 that *H. porcellanus* has a narrow distribution in the modern ocean. Specifically, this species
182 mainly occurs off Indonesia, Palau, and the Philippines for which the WOA2023 mean annual

Commented [DE10]: I added 'imposed' and deleted this as it doesn't make sense to talk about the sea surface or seasonality in culture.

Commented [DE11]: No need to cite it every time in my view

SST ranges between 27-31°C. *Hyatella arctica* (WS2) and *Tridonte borealis* (WS3) originate from the White Sea (Barents Sea) which, at the site of collection is characterised by a WOA2023 mean annual SST of 7.1°C (seasonal range 0.3-13°C) (. A $\delta^{18}O_{sw}$ value (VSMOW) of -3.8 ‰ was measured in situ. Bivalve *Tridacna squamosa* (TS2) grew in a large zoo aquarium with an average water temperature of 25.9°C and $\delta^{18}O_{sw}$ value (VSMOW) of -1.05 ‰ (Batenburg et al., 2011; Fursman et al., 2025).

Commented [DE12]: By whom? Us? If not, add a citation.

Commented [DE13]: Ten years of Tridacna sclerochemistry at up to daily resolution from a controlled aquarium environment–Records of habitat change, induced seasonality and growth variabilityM Fursman, V Warter, M Janse, W Renema, C Spötl, I Arndt, D Evans, ...
Palaeogeography, Palaeoclimatology, Palaeoecology, 113022

2.2 Eocene samples

Eocene samples were collected from the Barton Clay Formation (base of the Naish Member) at Barton-on-Sea (southern UK). Five specimens were analysed: the gastropods *Sycostoma* sp. (sample FG1), *Orthosurcula rostrata* (FG2), and *Strombus athleta* (FG3), and the bivalves *Bathytormus sulcata* (FM1) and *Arcturellina pusilla* (FM2). The samples were collected from the same location as sample SW1 examined by Evans et al. (2018) from the Hampshire Basin, but are of a slightly younger age (39.5-40.5 Ma).

All Eocene mollusc shells were determined to be >99% aragonite using powder X-ray diffraction (XRD).

2.3 Sample preparation

In the case of samples RM1, RM2, RG1, and RG2 the entire shell was crushed to sub-cm sized fragments and then ground to a powder using an agate mortar and pestle. For samples WS2 and WS3 material was taken from the inner shell layer avoiding the muscle scars, ventral margin and palial sinus, umbo and hinge. These shells were first cleaned by abrading the outer layer with a rotary drill bit operated at its lowest speed and pressure.

Samples CHA_M_050 and CHA_M_062 consist of bulk powder homogenised from *A. islandica* collected from NE Iceland in 2010 (Staudigel et al., 2023a; Pederson et al., 2019). Bulk powder was removed as circular cores from periodic growth bands using a drill, and were

subsequently homogenised with a mortar and pestle. Shell UH was analysed for fluid inclusion $\delta^{18}O$ prior to being homogenised, as described in Nooitgedacht et al. (2021).

In the case of TS2, a section was cut out of the inner shell layer and ground to a fine powder using an agate mortar and pestle.

Commented [DE14]: Do we want a one sentence paragraph?

The sample preparation for M2-Sf and M2-Sv is described in de Winter et al. (2021a). M2-Sf samples a sufficiently large portion of the shell to represent the mean annual temperature at which the specimen grew. M2-Sv is a sample that averages shell material formed throughout the second growth year of the specimen, although we note that growth rate might not be constant throughout the year.

In the case of cultured ME_002, ME_003, and AL_006 bulk shell parts were sampled without differentiated sampling of the outer and inner shell.

The Eocene samples FG1, FG2, FG3, FM1, and FM2 were crushed to smaller pieces using a hammer. These pieces were cleaned by scraping clay residues off with a spatula and rinsing the shell fragments with deionised (DI) water in an ultrasonic bath. They were ground to a powder in an agate mortar and pestle.

With the exception of samples RM1, RM2, RG1, and RG2, which were subjected to oxidative cleaning using a 3 wt.% NaOCl solution (Fiebig et al., 2024), the powders did not undergo any pre-treatment for organic matter removal. After reacting overnight, the NaOCl solution was discarded and the powders rinsed with DI water before being left to dry at room temperature for several days. All sample powders were stored in a vacuum dryer at 30°C before isotopic analysis. Non-bleached aliquots (n = 6) of RG2 were analysed along with bleached (n = 9) aliquots. We did not detect any significant differences (as in stats??) in the dual clumped isotope compositions for the two sets of sub-samples (see Supplementary Figure S1). Thus, we conclude that interfering components that release NO_2 (Fiebig et al., 2024) were absent, and that oxidative cleaning did not affect the dual clumped isotope compositions of our sample

powders. As such, both sub-sets of RG2 aliquots were pooled for the purpose of data interpretation.

2.4 Mass spectrometric analyses and data processing

All samples were analysed for their Δ_{47}, Δ_{48}, $\delta^{18}O$ and $\delta^{13}C$ values following the experimental setup of Fiebig et al. (2019) and methodology described by Bernecker et al. (2023). For dual clumped isotope measurements, 10 mg (±0.2 mg) per replicate were weighed into silver capsules, with 6-15 replicates were analysed for each sample. Acid digestion took place in a common acid bath at 90°C using phosphoric acid (>108 wt.%). ETH-1, ETH-2, non-bleached ETH-3, in-house Carrara marble as well as CO_2 gases equilibrated at 25°C and 1000°C, respectively, were analysed alongside the samples. The preparation process of equilibrated and heated gases followed the procedure described in Bernecker et al. (2023). All samples, standards, and gases were measured against a reference gas with the following isotopic compositions: $\delta^{13}C_{VPDB}$ = -4.2 ‰ and $\delta^{18}O_{VSMOW}$ = 25.26 ‰ (ISO-TOP, Air Liquide, France). Dual clumped data processing followed the method described in Bernecker et al. (2023), using optimal scaling factors for pressure baseline correction based on continuously monitored m/z 47.5 intensities and slope minimisation algorithm for δ^{47} vs. Δ_{47} and δ^{48} vs. Δ_{48} correlations of equilibrated gas data. Background corrected raw data was normalised to the Carbon Dioxide Equilibrium Scale for an acid digestion temperature of 90°C (CDES 90) (Dennis et al., 2011) using D47crunch (Daëron, 2021), pooling over all sessions and considering equilibrated gases as anchors exclusively. For this purpose, non-bleached replicates of ETH-3 were labelled individually in order to avoid any bias introduced by the variance algorithm of D47crunch (Fiebig et al., 2024). Reported uncertainties represent fully propagated 2 SE, considering allogenic and autogenic errors.

$\delta^{18}O$ values of carbonate samples analysed in this study were normalised against nominal values of ETH-1 and ETH-2 (Bernasconi et al., 2018). Since these ETH standards are calcite, the

difference in acid fractionation factors between aragonite (ar) and calcite (cc) at 90°C (Kim et al., 2007b) needs to be considered for the determination of aragonite $\delta^{18}O$. For this purpose, we considered equation (1):

$$\alpha_{CO_2-caCO_3} = \frac{\delta^{18}O_{CO_2}+1000}{\delta^{18}O_{CaCO_3}+1000} \quad (1)$$

For aragonitic samples, in a first step, $\delta^{18}O\text{-}CO_2$ was determined based on the $\delta^{18}O_{CaCO_3}$ normalised to ETH1 and ETH2, applying the acid fractionation factor ($\alpha_{CO_2-caCO_3}$) for calcite of 1.00813. In a second step, $\delta^{18}O\text{-}CO_2$ was inserted into equation (1) to determine the aragonitic $\delta^{18}O_{CaCO_3}$ using the aragonite-specific acid fractionation factor of 1.00854. For samples of mixed mineralogy (*P. vulgata, M. edulis*), we considered an effective acid fractionation factor α_{eff} that was weighted to the percentile abundances of calcite (x_{cc}) and aragonite ($1\text{-}x_{cc}$) in the sample to calculate $\delta^{18}O_{CaCO_3}$:

$$\alpha_{eff} = x_1\ \alpha_{CO_2-cc} + (1\text{-}x_{cc})\ \alpha_{CO_2-ar} \quad (2)$$

2.5 Dual clumped isotope equilibrium

In order to identify kinetic bias in the dual clumped isotope compositions of molluscs and to determine apparent growth temperatures we compare measured Δ_{47}-Δ_{48} values with the Δ_{47}-Δ_{48}-T relationships of Fiebig et al. (2024). The latter has been reprocessed from original highest precision data published by Fiebig et al. (2021) to exclude any bias from isobaric contamination of ETH3 (Fiebig et al., 2024). Over the temperature range of 8-1100°C, the reprocessed Δ_{47}-Δ_{48}-T relationships depart by less than -1 ppm (Δ_{47}) and -3 ppm (Δ_{48}) from the original relationships of Fiebig et al. (2021). The validity of the Δ_{47}-T and Δ_{48}-T relationships of Fiebig et al. (2021, 2024) have been independently confirmed by Anderson et al. (2021) and Swart et al. (2021), respectively. In the low temperature range, the Δ_{47}-Δ_{48}-T relationship of Fiebig et al.

(2024) is anchored against Devils Hole and Laghetto Basso carbonates. These two natural calcites were precipitated at extremely slow growth rates (< 1 µm/yr; Daëron et al., 2019), which brings them closest to the equilibrium limit of precipitation (Watkins et al., 2013, 2014) at which dissolution and precipitation rate of calcite become approximately equal. We therefore consider the Δ_{47}-Δ_{48}-T relationships of Fiebig et al. (2024) to reflect the most accurate and precise estimation of the position of Δ_{47}/Δ_{48} equilibrium that is currently available.

2.6 Re-evaluating the temperature dependence of the oxygen isotope fractionation between mollusc carbonate and water

We compiled on aragonite, calcite, and seawater $\delta^{18}O$ data from Grossman and Ku (1986), Lecuyer et al., (2004, 2012), Henkes et al. (2013), Caldarescu et al. (2021), Huyghe et al. (2022), and de Winter et al. (2022) to re-evaluate the temperature dependence of the oxygen isotope fractionation between mollusc shell-carbonate and seawater. We additionally included data from the modern specimens investigated here (Tables 1, 2), using directly measured temperatures for culture experiments and mean annual temperatures for naturally sampled specimens. The compiled data sets are available in Supplementary Table S1. Specimen-specific oxygen isotope data was considered in all cases. De Winter et al. (2022) originally provided high-resolution data from four specimens, so we calculated specimen-specific mean $\delta^{18}O$ values from their data in order to avoid over-representation. The aragonitic samples of Grossmann and Ku (1986) were acid digested at 50-60°C and calibrated against NBS 19 calcite. In order to account for the difference in acid fractionation factors between aragonite and calcite, we therefore considered the equation for acid fractionation for calcite by Kim et al. (2007b) (T = 55°C; $\alpha_{CO_2-cc} = 1.00919$) to calculate $\delta^{18}O_{CO_2}$ from the given $\delta^{18}O_{CaCO_3}$ and then their equation for aragonite (T = 55°C; $\alpha_{CO_2-ar} = 1.00955$) to obtain aragonitic $\delta^{18}O_{CaCO_3}$, as detailed in section 2.4. Oxygen isotope fractionation factors of aragonite and calcite with respect to water were calculated from published oxygen isotope compositions according to (3):

Commented [DE15]: I didn't understand this

$$\alpha_{CaCO_3-H_2O} = \frac{\delta^{18}O_{CaCO_3} + 1000}{\delta^{18}O_{H_2O} + 1000} \quad (3)$$

Uncertainties for oxygen isotope and temperature input data are not consistently reported in the studies of Grossman and Ku (1986), Lecuyer et al. (2004, 2012), Henkes et al. (2013), Caldarescu et al. (2021), Huyghe et al. (2022), and de Winter et al. (2022). An error-weighted linear regression would, therefore, add more weight to data that lacks any reported uncertainties, which needs to be avoided. Consequently, we did not consider uncertainties in compiled $\alpha_{CaCO_3-H_2O}$ values and growth temperatures in the computation of linear regressions.

3. Results

Bulk stable and clumped isotope compositions of all modern and fossil specimens analysed in this study are listed in Tables 3 and 4, respectively. Baseline-corrected input data (δ^{45}-δ^{49}) as well as Δ_{47}, Δ_{48}, $\delta^{18}O$, and $\delta^{13}C$ results, along with processing statistics, can be found in Supplementary Tables S2 and S3.

3.1 Clumped isotopes

Dual clumped isotope data of the molluscs are compared to the position of equilibrium (Fiebig et al., 2021, revised after Fiebig et al., 2024) in Figure 1 for modern samples and in Figure 2 for Eocene samples. With the exception of one specimen (RG2), all modern and Eocene molluscs plot indistinguishably from the Δ_{47}-Δ_{48} equilibrium line. Δ_{47}-derived temperatures obtained from modern and fossil specimen are listed in Table 2 and Table 4, respectively. A correlation plot of disequilibrium Δ_{47} vs disequilibrium Δ_{48} of modern specimens is provided in Supplementary Figure S2. Here, disequilibrium Δ_i corresponds to the difference between measured Δ_i and Δ_i predicted by habitat temperature based on the Δ_{47}-Δ_{48}-T relationship of Fiebig et al. (2024). Taking analytical and seasonal temperature variations into account, RG2 remains the only sample that plots outside of uncertainty from the expected range of equilibrium Δ_{47}-Δ_{48} values (Supplementary Figure S2).

331 Visual inspection of Figure 1 implies that samples in the lower temperature range, may, on
332 average, plot further from the equilibrium line than their higher temperature counterparts. In
333 order to quantitatively test if the dual clumped isotope composition of carbonate from
334 organisms characterised by relatively low mean annual growth temperatures (T < 10°C, group
335 1; n = 8) is characterised by a greater degree of scatter around the equilibrium line than those
336 grown at higher temperatures (T > 10°C, group 2; n = 8) we determined the absolute distance
337 of each data point from the equilibrium line. Namely, the absolute difference between measured
338 Δ_{48} and the Δ_{48} value displayed for the same sample by horizontal projection of its measured
339 Δ_{47} value to the equilibrium line. We then performed a t-test to investigate if the mean absolute
340 distance displayed by group 1 data is different to that derived from group 2. The t-test reveals
341 mean absolute distances of 16.1 ± 1.6 ppm (1 SE) and 4.6 ± 1.3 ppm for group 1 and group 2,
342 respectively. A p-value of 0.0003 indicates the two populations are distinguishable from each
343 other, highlighting that organisms with growth temperatures <10°C exhibit significantly larger
344 departures from the Δ_{47}-Δ_{48} equilibrium line than those living in warmer water masses (T >
345 10°C).

Commented [DE16]: 'is' is correct (mean absolute distance is singular)

346 3.2 Oxygen isotope fractionation between water and carbonate

347 1000lnα($CaCO_3$-H_2O)-1/T relationships for aragonite and calcite are displayed in Figure 3a and
348 3b, respectively, yielding the following equations 4 and 5:

$$\text{Aragonite:} \quad 1000\ln(\alpha) = 16.438\ (\pm 0.424) \times (10^3/T) - 25.77\ (\pm 1.46), \quad (4)$$
$$R^2 = 0.90,\ n = 154$$

$$\text{Calcite:} \quad 1000\ln(\alpha) = 15.663\ (\pm 0.832) \times (10^3/T) - 23.62\ (\pm 2.87), \quad (5)$$
$$R^2 = 0.81,\ n = 81$$

349 In order to constrain the sensitivity of the regressions to possible outliers in the two data sets,
350 we compare the above ordinary least-squares regression to those resulting from a bootstrapping
351 approach, in which the individual data sets were randomly resampled 10000 times, adding

higher weight to random individual samples by resampling with replacement. Each outcome was fit using ordinary least-squares regression again. The overall results, based on the 50th percentile of the 10^4 regression coefficients, are shown in Supplementary Figure S3. These demonstrate that the difference between the original and resampled approach results in calibrations that differ by less than 0.12 ‰ across the entire investigated temperature range.

4. Discussion

4.1 Dual clumped isotope thermometry on modern mollusc shells

Although most modern samples have dual clumped isotope compositions that fall within uncertainty of equilibrium, this observation, on its own, does not provide unambiguous evidence that equilibrium has been attained in each case. A comparison of measured growth temperatures with Δ_{47}-derived growth temperatures is necessary to prove this hypothesis in more detail. This comparison allows us to identify samples that have been affected by two or more rate-limiting kinetic processes which – in combination – could lead to Δ_{47} and Δ_{48} values plotting fortuitously indistinguishably from equilibrium, as was observed for individual brachiopods (Davies et al., 2023).

Δ_{47}-derived temperatures for samples *B. undatum* (RG1), *M. modiolus* (RM1) and *S. solida* (RM2), which are apparently in equilibrium (Fig. 1), are 6.8°C (±2.2°C, 95CI), 8.2°C (±2.3°C) and 8.2°C (±2.4°C), respectively. These values agree with the mean annual sea surface temperature (MASST) of 9.6°C and/or the seasonally monitored temperature range of 7.0-12.4°C reported for the beach at Tentsmuir Forest within their errors (Table 2, Supplementary Figure S2). A fourth sample, *P. vulgata* (RG2) was collected at the same sample location. Its Δ_{47}-derived temperature of 9.1°C (±1.6°C) is consistent with the MASST of 9.7°C (Table 2); however, its Δ_{48}-value exhibits a slightly positive, but significant bias relative to the equilibrium Δ_{48}-value expected for this temperature (Fig. 1; Supplementary Figure S2). Fiebig et al. (2024) found that NO_2 interferent can cause -Δ_{47}/+Δ_{48} offsets from equilibrium, but NO_2 bias can be

excluded in this case since the mean Δ_{47} and Δ_{48} values of bleached and unbleached aliquots of that sample were indistinguishable from each other (Supplementary Figure S1). The outer and inner shell areas of bivalve RG2 consist of calcite and aragonite, respectively; such that our powder sample is of mixed mineralogy. The $\delta^{18}O$ values of both phases, however, differ by less than 1‰ such that non-linear mixing also cannot explain the observed offset from equilibrium (Staudigel et al., 2023a, b; White & Defliese, 2023). Since artificial biases like mixing and NO_2 interference can be excluded, the observed disequilibrium signature of RG2 may, therefore, be of a kinetic nature that needs to be explored in more detail.

Δ_{47}-derived temperatures for all three specimens of *A. islandica* (AL_006, CHA_M_050, and CHA_M_062), all of which plot indistinguishably from equilibrium (Fig. 1), align with the independently known growth temperature ranges (Table 2; Supplementary Figure S2). In the case of AL_006, which was grown in culture at a constant temperature of 12.0°C, we reconstruct a temperature of 12.3°C (±2.3°C). CHA_M_050 and CHA_M_062 were collected from the NE Iceland margin alongside molluscs analysed in Pederson et al. (2019). The Δ_{47}-derived temperatures for these samples are 7.6°C (±2.3°C) and 5.1°C (±2.3°C), respectively. A mean annual water temperature of 3.9°C was estimated for the site of sample collection, although the summer temperature at this location can reach 7.4°C (Table 2). We therefore conclude the most likely explanation for this offset towards warmer temperature reconstructions may be due to preferential shell growth during summer months as observed for some molluscs (e.g., Vitahkari et al., 2016; Witbaard et al., 1994; Goodwin et al., 2001; Kaandorp et al., 2003; Judd et al., 2017; de Winter et al., 2021a, b).

The sampled parts of the mussels *M. edulis* ME_002 and ME_003 were cultured at 5-25°C with a mean temperature of 16.2°C. Although temperature was briefly raised to 31°C and lowered to 3°C over a short period of time for the purpose of conducting respiration rate experiments (Jansen et al., 2007). Δ_{47}-derived temperatures for ME_002 and ME_003 are 16.1°C (±2.2°C) and 15.4°C (±2.3°C), respectively (Table 2), aligning well with estimated mean growth

404 temperatures and, therefore, confirm that dual clumped isotope equilibrium has been attained
405 (Fig. 1; Supplementary Figure S2).
406 Samples of the oyster *M. gigas* (M2-Sf and M2-Sv) also plot indistinguishably from the
407 equilibrium line within uncertainty (Fig. 1). These samples were taken from the same oyster
408 shell. Measured Δ_{47}-values correspond to temperatures of 19.0°C (±2.2°C) and 11.9°C
409 (±2.0°C), respectively (Table 2). The sample powders originate from two different small areas
410 of the shell with different microstructures, i.e., from the foliated calcite in the hinge (M2-Sf)
411 and from the chalky calcite material of the second growth year (M2-Sv) (see de Winter et al.,
412 2021a, b for more information). Both sample powders represent averages of material
413 precipitated across seasons, with their Δ_{47}-derived temperatures therefore potentially
414 representing either mean annual or seasonal temperature, depending on when growth occurred
415 (seasonal range of growth temperatures: 4.5-19.2°C, mean: 11.5°C, Table 2). M2-Sf exhibits a
416 Δ_{47} temperature that corresponds to the maximum seasonal temperature. The colder Δ_{47}-derived
417 formation temperature of 11.9°C (±2.0°C) for M2-Sv, on the contrary, is in excellent agreement
418 with the measured mean annual temperature of 11.5°C. The different temperatures obtained for
419 M2-Sf and M2-Sv might stem from sampling bias. Given that the two samples are from the
420 same species a different calcification response to temperature change would not be expected.
421 Instead, considering that only small areas were sampled, it is more likely that the powders
422 represent different seasonal stages of growth.
423 Three *Tridacninae* from both the natural environment and an aquarium, including two different
424 species, were analysed. The samples from a specimen of *H. porcellanus* (Shell UC and Shell
425 UH) plot indistinguishably from the equilibrium line (Fig. 1) and yield Δ_{47}-derived growth
426 temperatures of 26.4°C (±2.3°C) and 28.3°C (±2.2°C), respectively (Table 2). These
427 temperatures match independently constrained habitat temperatures of 27-31°C. *T. squamosa*
428 (TS2), which also plots within uncertainty indistinguishably from the equilibrium line (Fig. 1),
429 was cultured in an aquarium kept at near-constant temperature. The Δ_{47}-derived temperature of

24.4°C (±2.2°C) agrees with the mean growth temperature of 25.9°C (up to 26.8°C during summer) (Batenburg et al., 2011; Janse et al., 2008) within uncertainty (Table 2).

H. arctica (WS2) and *T. borealis* (WS3) from the White Sea plot above albeit within uncertainty of the equilibrium line (Fig. 1). The Δ_{47}-derived temperature of 8.3°C (±2.0°C) for WS3 agrees within error with the estimated MASST of 7.1°C (Table 2). WS2 intersects the equilibrium line at its lower boundary level of Δ_{47} uncertainty. This intersection reflects a temperature of 3.2°C, lower than MASST but within the range of seasonal surface temperatures characteristic of the White Sea (0.3 – 13°C; Table 2). Supplementary Figure S2 confirms that WS2 plots indistinguishably from equilibrium if seasonal temperature bias and growth are considered.

Overall, most specimens that have dual clumped isotope compositions indistinguishable from equilibrium are characterised by Δ_{47}-derived temperatures that are in good agreement with observed (seasonal) growth temperatures. This strongly implies that the internal arrangement of heavy isotopes during $CaCO_3$ precipitation often proceeds up to equilibrium. Bulk mollusc shell samples may, therefore, provide a robust archive for accurate and highly precise temperature reconstructions by means of Δ_{47} thermometry. Potential seasonal biases due to preferential growth during summer need to be considered, especially when analysing bulk shells from mid-high latitude regions. At relatively low growth temperatures <10°C, kinetic limitations may become increasingly relevant. In this temperature range, mean Δ_{48} values depart significantly farther from the equilibrium line than at T >10°C (see section 3.1), and one out of eight specimen exhibits disequilibrium dual clumped isotope signatures. A more detailed investigation on multiple specimens per species and different growth increments are necessary to confirm that disequilibrium Δ_{47} and Δ_{48} patterns in molluscs occur more often in the low temperature range. Until proven otherwise, care should be taken if Δ_{47} indicates temperatures <10°C, and, if possible, Δ_{48} be analysed along with Δ_{47} in order to identify potential kinetic bias.

455 **4.2 Key parameters affecting biomineralisation of molluscs**

456 Our observation that most of the investigated bivalve molluscs form their shells close to
457 equilibrium differs from what is known about several other marine calcifying organisms. For
458 example, corals exhibit disequilibrium dual clumped isotope compositions, which has been
459 proposed to be the result of CO_2 absorption during biomineralisation (Bajnai et al., 2020;
460 Davies et al., 2022). Corals actively elevate the pH at their site of calcification (SOC) above
461 that of ambient seawater, due to addition of Ca^{2+} or Na^{+} into the calcifying fluid and charge-
462 balance-removal of H^{+} (e.g.; Spooner et al., 2016; Venn et al., 2019). During this process,
463 aqueous CO_2 from ambient seawater and/or the ambient tissue cells diffuses into the SOC along
464 its concentration gradient. At the SOC, this CO_2 is then transformed into bicarbonate via
465 hydration/hydroxylation. These two reactions and their reverse reactions,
466 dehydration/dehydroxylation, can be rate-limiting in the DIC-water-$CaCO_3$ system, and,
467 therefore, in the accompanying oxygen isotope exchange among the different DIC species and
468 water (McConnaughey, 1989b; Adkins et al., 2003; Sade and Halevy, 2017; Affek, 2013; Guo
469 2020). Protonation/deprotonation of carbonate/bicarbonate, on the contrary, occurs almost
470 instantaneously such that metastable chemical and isotopic equilibrium between both species
471 is obtained at any time (McConnaughey, 1989b; Adkins et al., 2003; Chen et al. 2018).
472 Achieving oxygen and clumped isotope equilibrium in the DIC-H_2O system thus depends on
473 the relative rates of CO_2 hydration/hydroxylation, bicarbonate dehydration/dehydroxylation
474 and precipitation. If precipitation proceeds faster than isotopic equilibration of the DIC pool,
475 disequilibrium signatures will be recorded in the forming carbonate (e.g., McConnaughey,
476 1989b; Adkins et al., 2003; Chen et al. 2018; Guo & Zhou, 2019; Guo, 2020; Bajnai et al.,
477 2020). In the case of cold and warm water corals, the dehydration/dehydroxylation reactions
478 are slowest such that the isotopic composition of the precipitated carbonate largely records the
479 kinetic isotope effects associated with the hydration/hydroxylation reactions of CO_2, resulting
480 in lighter-than-equilibrium $\delta^{18}O$, $\delta^{13}C$, and Δ_{48} values, but heavier Δ_{47} (Davies et al., 2022).

In the case of molluscs, the extrapallial fluid (EPF), in which precipitation takes place, is enclosed by the calcifying cells of the mantle epithelium as well as the periostracum, an organic layer covering the shell and extending over its edge (Fig. 4). The intra-cellular pH of the mantle cells is known to be around 7.4-7.5, while the EPF is characterised by a pH of ~7.8 (Ip et al., 2006) but may be as low as 7.2 (Crenshaw, 1972). The cytosol of the surrounding cells are slightly more acidic than the EPF, which will result in diffusion of (metabolic) CO_2 from the surrounding cells into the EPF. The rate of (de)hydration/(de)hydroxylation reactions, and thus the rate at which isotopic equilibration of the DIC-H_2O system is achieved, is largely affected by factors such as pH and temperature, with higher pH and lower temperatures resulting in slower isotopic equilibration rates (e.g., Guo, 2020). The rate-dependence of the attainment of equilibrium on pH might offer an explanation for why molluscan shell carbonates exhibit equilibrium dual clumped isotope compositions while skeletons of corals do not. Unlike corals, which elevate the pH at the SOC above seawater pH to initiate calcification, the pH of the EPF is lower than that of seawater (which in molluscs is the equivalent to the SOC in corals) by 0.5-0.6 units (cf. Crenshaw, 1972). At 25°C, isotopic equilibration of the DIC-H_2O system at a pH of 7.7 is predicted to proceed five times faster than at a pH of 8.7 that likely prevails at the SOC of some corals (e.g., Ross et al., 2022 and references therein) (Guo, 2020). At 10°C and 5°C, on the contrary, the overall equilibration rate at a pH of 7.7 is reduced by a factor of 3 and 5, respectively, relative to 25°C. The absolute rate of equilibration furthermore depends on the absence/presence of the enzyme carbonic anhydrase (CA). CA catalyses the hydration of CO_2 (e.g., Freeman & Wilbur, 1948; Nielsen and Frieden, 1972; Uchikawa and Zeebe, 2012; Le Roy et al., 2016) using Zn^{2+} as central ion in order to polarise, and therefore activate, water for the reaction (Park & Lee, 2019). The presence of CA has been observed in both corals (e.g., Uchikawa and Zeebe, 2012; Bertucci et al., 2013) and molluscs (e.g., Freeman and Wilbur, 1948; Nielsen and Frieden, 1972). CA has been found to be directly involved in molluscan shell formation, e.g., in the matrix during nacre production (Marie et al., 2008), as a domain in

Commented [PS17]: Joji Uchikawa has some lovely papers that say this. I would suggest also referencing Uchikawa and Zeebe (2012); carbonic anhydrase… Beck et al., (2005) is another good reference for these kinetics.

nacrein (a protein important for nacre-formation) (Miyamoto et al., 1996) as well as in the mantle cells (Cardoso et al., 2019). In molluscs, proteins like nacrein inhibit calcium carbonate crystallisation from supersaturated solutions (Miyamoto et al., 2005), possibly to enable the organisms to tightly control the rate of calcification. In addition to pH and temperature, the presence of CA and nacrein may, therefore, act to result in the attainment of equilibrium in the molluscan DIC-H_2O-$CaCO_3$-system.

4.3 Kinetic biases and the potential impact of sample habitat

Increased scatter around the Δ_{47}-Δ_{48} equilibrium line at temperatures <10°C may indicate that (de)hydration/(de)hydroxylation reactions slowly become rate-limiting at low temperatures. CO_2-absorption is known to introduce $+\Delta_{47}/-\Delta_{48}$ offsets from dual clumped isotope equilibrium and has been shown to be of importance in other biogenic carbonates such as corals and brachiopods (Davies et al., 2022; Davies et al., 2023). CO_2 degassing, on the contrary, goes along with $-\Delta_{47}/+\Delta_{48}$ offsets from equilibrium and have been postulated to be effective in bivalve molluscs (Curley et al., 2023).

A single measured sample (*P. vulgata*; RG2) plots below the equilibrium line in dual clumped isotope space (Fig. 1). Its Δ_{47} value, however, corresponds to MASST at its growth site (Table 2). *P. vulgata*, a common limpet occupying an intertidal habitat, is submerged at high tides and exposed to air at low tides. Gas exchange with the surrounding environment during times of emersion is restricted in order to prevent desiccation (e.g., Burnett, 1988). To counteract the resulting hypercapnia (i.e., the accumulation of metabolic CO_2 which leads to acidification of the haemolymph) parts of the (inner) shell are dissolved (Lindinger et al., 1984). During this process, the DIC concentration of the EPF thus increases. It has been postulated that CO_2-degassing might occur as soon as the mollusc is submerged again and gas exchange with the surrounding water resumes (Curley et al., 2023). It has also been postulated that calcification rates in intertidally living species are accelerated during times of submersion (Tagliarolo et al., 2013a, b) but cease during emersion. This acceleration of growth rate may be explicable by the

Commented [DE18]: This sounds like this is something that they're trying to achieve, whereas it is a result of controlling another process

Commented [DE19]: The idea in Curley et al. is really interesting and I agree it could/should be mentioned here. This needs some explanation though - in the previous section you describe CO2 absorption into the EPF due to the low cytosolic pH, so suddenly suggesting the opposite here will be confusing to anyone who hasn't read that paper.
At the very least, this needs some further explanation/introduction.

Commented [DE20]: Here you do explain CO2 degassing, in which case the simplest change in response to my previous comment would be to delete the last sentence in the previous paragraph (after '…Davies 2022;2023)' as you already reference Curley et al. here.

Commented [PS21]: Perhaps chose a word that doesn't have a homophone that is it's opposite? Emersion and immersion sound the same, but mean opposite things. Emergence, maybe? Or just "low tide"?

fact that the organism is in contact with seawater, from which the ions for calcification are ultimately derived, for less time than subtidal species, of relevance because an accelerated growth rate in combination with CO_2 degassing may result in disequilibrium bias. In addition, amorphous calcium carbonate (ACC) has been observed in some species (Weiss et al., 2002; Nassif et al., 2005; Jacob et al., 2011), representing a transient precursor of more stable crystalline aragonite or calcite (see e.g., Addadi et al., 2003, 2006). Tagliavento et al. (2023) showed that high Mg-calcite formed via ACMC, exhibited a significant $+\Delta_{48}$ bias relative to the Δ_{48} calcite equilibrium value predicted by its formation temperature, whereas its Δ_{47} corresponded to that temperature. The positive Δ_{48} disequilibrium bias of RG2 may, therefore, imply that ACC is involved in the biomineralisation process of *P. vulgata*. If so, the absence of such a bias in *M. edulis* (samples ME_002 and ME_003), in which aragonite and calcite production has been shown to proceed via ACC (Fitzer et al., 2016), would indicate that the $+\Delta_{48}$ bias of ACC can be subsequently overprinted during its transformation to the final polymorph.

Based on the analysis of a single specimen we cannot identify which process is responsible for the apparent disequilibrium signal in RG2. It should also be borne in mind that one of the ~20 samples reported here is statistically expected to fall outside of uncertainty of the dual clumped isotope equilibrium line based on its fully propagated 95% confidence interval. More dual clumped isotope data on intertidal species is required to investigate if their isotopic compositions are affected by kinetic isotope effects. While *M. gigas* as well as *M. edulis* also occur in intertidal habitats and therefore could help resolve this issue, there were no tidal cycles present during the time period of culture experiments in which these specimens were grown. Future studies using dual clumped isotopes should also confirm whether kinetic limitations occur in the inner shell layer, as postulated previously (Curley et al., 2023).

4.4 Oxygen isotope fractionation into aragonitic and calcitic mollusc shells

558 It is still unknown if, and to what extent, the temperature dependence of equilibrium oxygen
559 isotope fractionation between aragonite and water differs from that between calcite and water.
560 Attempts to determine such equilibrium relationships have been made using inorganic
561 precipitation under controlled conditions (e.g., Kim & O'Neil, 1997; Kim et al., 2007a; Dietzel
562 et al., 2009; Watkins et al., 2013; Wang et al., 2013) and through theoretical calculations (e.g.,
563 Schauble et al., 2006; Hill et al., 2014), although these theoretical computations yielded
564 inconsistent results. Whereas Hill et al. (2014) predicted a 1.3 ‰ fractionation in $\delta^{18}O$ values
565 between aragonite and calcite at 25°C, the results of Schauble et al. (2006) suggest no
566 significant fractionation between these two minerals at the same temperature. Inorganic
567 precipitation experiments revealed that the oxygen isotope fractionation between calcite and
568 water can vary with pH (due to the kinetic isotope effects (KIEs) associated with CO_2-
569 bicarbonate interconversion) and precipitation rate (e.g., Dietzel et al., 2009). While Kim &
570 O'Neil (1997) proposed an equilibrium $1000\ln\alpha(\text{calcite-}H_2O)$-1/T relationship, they achieved
571 supersaturation and calcite precipitation via the continuous removal of CO_2 from Na-Ca-HCO_3^-
572 solutions and did not report if oxygen isotope equilibrium between DIC species and water was
573 attained prior to the onset of precipitation. In addition, that study precipitated $CaCO_3$ along a
574 pH gradient in the absence of carbonic anhydrase at rates which are insufficient to maintain
575 oxygen isotope equilibrium in the $CaCO_3$-DIC-H_2O system during progressive precipitation
576 (Watkins et al., 2014).
577 It is now widely accepted that the indistinguishable $1000\ln\alpha(\text{calcite-}H_2O)$-1/T relationships of
578 Coplen (2007) and Däeron et al. (2019) are closest to equilibrium. These relationships were
579 derived from natural subaqueous calcites that precipitated at extremely low rates (<1 µm/yr) at
580 which the dissolution rate approaches the precipitation rate (Watkins et al., 2013, 2014). In the
581 temperature range of 0-40°C, the $1000\ln\alpha$-1/T relationship of Coplen (2007) differs from the
582 aragonite equilibrium relationship proposed by Kim et al. (2007a) by 0.8 to 1.0 ‰. It remains
583 unclear if oxygen isotope equilibrium has been attained in the aragonite precipitation

Commented [MB22]: You mostly used 1000lna(CaCO3-H2O)

experiments of Kim et al. (2007), with the above observation suggesting that this was not the case. Aragonite is metastable at ambient temperatures, and calcite precipitation was kinetically inhibited via the addition of Mg^{2+}.

There is currently no indication from clumped isotope measurements that aragonite and calcite exhibit different states of equilibrium with respect to temperature (e.g., Defliese et al., 2015; de Winter et al., 2022; Bernecker et al., 2025). Our results support these previous findings. With the exception of RG2, M2-Sf, M2-Sv, ME_002 and ME_003, all other molluscs analyses presented here are entirely composed of aragonite. These aragonitic specimens exhibit dual clumped isotope compositions that are indistinguishable from the inorganic calcite equilibrium-Δ_{47}-Δ_{48}-T relationship (Fig. 1). Moreover, their Δ_{47} values correspond to independently constrained habitat temperatures (see section 4.1).

To investigate potential differences in mollusc-specific $1000\ln\alpha(CaCO_3\text{-}H_2O)\text{-}1/T$ relationships we compiled the available datasets for aragonite (Fig. 3a) and calcite (Fig. 3b). Linear regressions obtained on these two datasets are compared to the inorganic calcite-water relationships of Coplen (2007) and Kim & O'Neil (1997), and to the inorganic aragonite-water relationship of Kim et al. (2007a) in Figure 3c. We find that calcitic molluscs exhibit oxygen isotope fractionations closer to the equilibrium fractionation of Coplen (2007) at warmer temperatures (Fig. 3c). On the contrary, at colder temperatures, the molluscan calcite fractionation line approaches the (kinetically biased) regression line published by Kim and O'Neil (1997).

Over the investigated range of 0-40°C, at any given T, the oxygen isotope fractionation between aragonitic molluscs and seawater is 0.5 to 1.0 ‰ larger than that between calcitic molluscs and seawater (Fig. 3c). Aragonitic molluscs display the same behaviour as their calcitic counterparts; the corresponding oxygen isotope fractionations approach values predicted by Coplen (2007) at the upper end of the temperature range covered by the data (~30°C), but

Commented [DE23]: Right?

Commented [DE24]: It wasn't clear to me whether this is a more general observation or specifically about Kim et al.

Commented [DE25]: On re-reading, I don't understand what 'different states' means. Do you mean whether the position of equilibrium differs for calcite and aragonite? Please clarify.

609 increasingly deviate from the latter with decreasing temperature, approaching the experimental
610 aragonite relationship published by Kim et al. (2007a) at 0°C.
611 Our observation that the oxygen isotope fractionation between aragonite and water approaches
612 values predicted by Coplen (2007) at elevated temperatures may indicate that aragonite and
613 calcite share the same $1000\ln\alpha(CaCO_3\text{-}H_2O)\text{-}1/T$ equilibrium relationship, but that the
614 attainment of isotopic equilibrium with water is kinetically inhibited at common Earth-surface
615 temperatures. The observed differences in the magnitude of oxygen isotope fractionation
616 between aragonite and calcite might be due to small differences in KIEs prevalent at the
617 mineral-fluid interface during mineral formation. These interfacial KIEs might differ in extent
618 depending on the forming polymorph, for example, because detachment/attachment kinetics
619 (Watkins et al., 2013; 2014) may depend on the characteristics of the mineral surface which, in
620 turn, may depend on the respective polymorph that is forming. Alternatively, the high level of
621 supersaturation required for aragonite precipitation may, for a given pH and temperature,
622 proceed with faster interconversion between dissolved CO_2 and bicarbonate.
623 Above a temperature of 10°C, at which kinetic departures from Δ_{47} and Δ_{48} equilibrium values
624 may become inconsequential (Fig. 1), our empirical mollusc-specific $1000\ln\alpha(CaCO_3\text{-}H_2O)\text{-}$
625 1/T relationships for aragonite and calcite depart from that of Coplen (2007) by up to -0.5 ‰
626 and -1.2 ‰, respectively (Fig. 3c). It was noticed in several studies that the Δ_{47} composition of
627 carbonate precipitates did not correlate with the oxygen isotope fractionation between carbonate
628 and water if this fractionation deviated from that predicted by Coplen (2007) by less than -1.5
629 ‰ (e.g., Kelson et al., 2017; Levitt et al., 2018; Jautzy et al., 2020; Fiebig et al., 2021). The
630 observed discrepant behaviour between clumped and oxygen isotopes may support the
631 hypothesis that interfacial isotopic equilibration occurs faster for clumped than for oxygen
632 isotopes (Tripati et al., 2015; Levitt et al., 2018), such that there exists a precipitation regime
633 where DIC disequilibrium is exclusively recorded in the oxygen isotope composition of the
634 precipitated carbonate. Alternatively, it may simply indicate that disequilibrium is analytically

635 better resolvable using oxygen isotopes, i.e., relative to the extent of disequilibrium, the
636 analytical uncertainty is smaller for oxygen than for clumped isotopes.

637 **4.5 Application to fossil material – temperature and $\delta^{18}O_{sw}$ reconstructions for the mid-**
638 **Eocene**

639 Our modern mollusc shell data provide evidence that these carbonates represent robust archives
640 for accurate and highly precise paleo-temperature reconstructions by means of exclusive Δ_{47}
641 measurements, without the need for a mollusc-specific calibration relationship. As long as
642 kinetic isotope effects are absent, uncertainties in reconstructed temperatures are exclusively
643 defined by the analytical uncertainty of Δ_{47} measurements. To test whether disequilibrium
644 effects are similarly absent in fossil material, the dual clumped isotope signature of five Eocene
645 mollusc shells collected from the same bed were measured. All investigated fossil samples,
646 consisting of five different species, correspond to dual clumped isotope equilibrium within the
647 uncertainty of the measurements (Fig. 2). Δ_{47}-derived temperatures are 17.3°C (±2.3°C, 95CI)
648 for FG1, 20.5°C (±2.3°C) for FG2, 20.3°C (±2.3°C) for FG3, 20.7°C (±2.4°C) for FM1, and
649 23.2°C (±2.3°C) for FM2 (Table 4). A temperature of 23.3°C (±5.0°C, 2SD) has been obtained
650 on an older sample (42.5 Ma versus 39 Ma) from the Hampshire Basin (Evans et al., 2018),
651 based on Δ_{47} analysis of a shallow-dwelling (symbiont-bearing) large benthic foraminifera.
652 Marchegiano and John (2022) reported a temperature range of 15-23°C based on Δ_{47} analysis
653 of gastropods from the Naish Member of the Barton Clay Formation – the same member as our
654 samples. The geologically-rapid evolution of the paleo-geography of this region in the (mid)
655 Eocene (Clark et al., 2022; Kniest et al., 2024b) means that we cannot unambiguously ascribe
656 the cooler mollusc versus foraminifera-derived temperatures to a changing global climate
657 versus differences in habitat or seasonal growth pattersn (although these are nonetheless within
658 uncertainty of each other). However, we note that this is consistent with Eocene global cooling
659 in the North Atlantic (Bijl et al., 2009; Inglis et al., 2015, 2023).

660 Insertion of Δ_{47} derived temperatures in equation (4) yields seawater $\delta^{18}O$ values between -3.5
661 ‰ and -2.3 ‰ for the mid Eocene (Table 4). These low and variable $\delta^{18}O$ seawater values agree
662 well with those reconstructed for the Hampshire Basin, in the southern part of the North Sea,
663 and the Paris Basin, based on a combination of $\delta^{18}O_{carb}$ and Δ_{47} data. Evans et al. (2018)
664 analysed foraminiferal calcite from the Hampshire Basin and reported a $\delta^{18}O$ seawater value of
665 -4.14‰ for an age of 42.5 Ma. Marchegiano and John (2022) analysed gastropods from the
666 Bartonian in the Hampshire Basin and reconstructed $\delta^{18}O$ seawater values for the Naish
667 Member of the Barton Clay Formation ranged from -1 to -2.5 ‰. Kniest et al. (2024a),
668 analysing a 40 Ma old bivalve mollusc shell, reconstructed $\delta^{18}O$ seawater values of -0.9 ‰ to -
669 2.7 ‰ for the Paris Basin, ascribing this substantial spatiotemporal seawater $\delta^{18}O$ variation to
670 different degrees of freshwater input through space and time. Kniest et al. (2024b), by means
671 of Ba/Ca and $^{87}Sr/^{86}Sr$ analysis of Eocene bivalves (genera *Venericor* and *Crassatella*),
672 independently confirmed substantial freshwater fluxes into parts of the Hampshire Basin during
673 the mid-Eocene. Finally, variable and negative seawater $\delta^{18}O$ values of about -2 ‰ have also
674 been reported for the early Bartonian in the southern part of the North Sea (De Man et al., 2004).
675 Altogether, our and these previous studies contribute to a coherent picture of relatively negative
676 and variable seawater $\delta^{18}O$ values in this region during the mid-late Eocene. The driver of this
677 has been suggested to be the local hydrographic regime (Kniest et al., 2024b), in particular the
678 relatively enclosed nature of at least parts of this basin during some intervals of the Eocene,
679 coupled with river-derived freshwater input to the relatively nearshore environments the source
680 of many samples.

681 **5. Conclusions**

682 We used dual clumped isotope thermometry to demonstrate that the bulk shell of molluscs may
683 constitute a promising archive for accurate and highly precise temperature reconstructions using
684 the Δ_{47} proxy. The majority of the specimens analysed here (15/16 modern and all fossil

samples) plot indistinguishably from dual clumped isotope equilibrium, while their corresponding Δ_{47} values correspond within uncertainty to independently constrained habitat temperatures. Kinetic biases may become important at temperatures <10°C, but more detailed investigations are necessary to verify this hypothesis. We ascribe the absence of significant kinetic isotope effects in the clumped isotope composition to precipitation from a closely equilibrated DIC pool. Close attainment of isotopic equilibrium in the DIC pool is facilitated by the relatively low pH (~7.6-7.8) of the EPF, compared to other marine calcifiers such as corals, and utilisation of carbonic anhydrase.

In addition, we present revised empirical relationships for the temperature dependence of oxygen isotope fractionation between molluscan aragonite/calcite and water, integrated over multiple species and datasets. At relatively high temperatures, both relationships become indistinguishable from the proposed calcite-water equilibrium relationship of Coplen (2007) suggesting that calcite and aragonite may have identical states of equilibrium, but that low bulk oxygen isotope equilibrium is typically not obtained at low temperatures. At these temperatures, oxygen isotopes seem to be more prone to disequilibrium effects than clumped isotopes.

Finally, we showed that a set of well-preserved Eocene mollusc samples are also characterised by equilibrium dual clumped isotope compositions. Using Δ_{47} data to reconstruct temperature and $\delta^{18}O_{sw}$ of the Hampshire Basin (UK) at ~39 Ma, we show that five different species are characterised by temperatures of 17.3-23.2°C, all of which are within uncertainty of each other. Reconstructed seawater $\delta^{18}O$ values of -3.5 to -2.3 ‰ agree well with previous estimates, adding to a body of evidence that suggests substantial (seasonal) freshwater input to at least parts of this basin during this time.

Acknowledgments

We thank C. Renker and M. Grimm for the identification of fossil and modern species analysed in this study. Sven Hofmann, M. Tagliavento and M. Schumann are acknowledged for their support during clumped isotope analysis. R. Petschick kindly provided XRD measurements. Aleksandra Bitner is thanked for providing White Sea mollusc specimens, Max Janse for providing the *T. squamosa* specimen, and Rob Witbaard is thanked for providing *Mytilus edulis* specimens. This work was enabled through FI-948/13-1 granted to JF through the Koselleck-programme of the DFG. JF, AD, DE and WM also acknowledge funding through the VeWA consortium by the LOEWE program of the Hessen Ministry of Higher Education, Research and the Arts, Germany. NJW is supported by the Dutch Science Foundation (NOW) through a VENI fellowship (Grant nr. VI. Veni.222.354) and through the FWO Climate Prize by the Flemish Research Council. DE additionally acknowledges support from the Volkswagen Stiftung *Experiment!* initiative (award reference: A131440). Further, WM and JF acknowledge DFG-funding through MU 3739/6-1 and FI-948/15-1, respectively.

CRediT statement

Schlidt Vanessa: Conceptualization, Methodology, Validation, Formal analysis, Investigation, Data Curation, Writing - Original Draft, Writing - Review & Editing, Visualization, Project administration. **Evans David**: Methodology, Formal analysis, Investigation, Resources, Writing - Original Draft, Writing - Review & Editing, Visualization, Supervision, Project administration, Funding acquisition. **de Winter Niels**: Validation, Investigation, Resources, Writing - Original Draft, Writing - Review & Editing, Funding acquisition. **Bernecker Miguel**: Methodology, Software, Investigation, Data Curation, Writing - Original Draft, Writing - Review & Editing. **Arndt Iris**: Investigation, Resources, Writing - Original Draft. **Staudigel Philip**: Investigation, Writing - Original Draft. **Davies Amelia**: Investigation, Writing - Original Draft. **Brand Uwe**: Resources, Writing - Original Draft. **Müller Wolfgang**: Resources, Writing - Original Draft, Funding acquisition. **Fiebig Jens**: Conceptualization,

Methodology, Validation, Investigation, Resources, Data Curation, Writing - Original Draft, Writing - Review & Editing, Supervision, Project administration, Funding acquisition.

Appendix A. Supplementary Material

Supplementary Figure S1 provides a comparison of Δ_{47}/Δ_{48} values of unbleached (RG2_U), bleached RG2* and pooled RG2.

Supplementary Figure S2 displays to which extent measured Δ_{47} and Δ_{48} values depart from expected equilibrium Δ_{47} and Δ_{48} values. For such a graphical illustration, two sources of uncertainties need to be considered: 1) Δ_i values have an analytical uncertainty, $d\Delta_i$, that corresponds to fully error propagated 2SE. 2) For a given organism, growth temperature might have occurred at any temperature within the seasonal range provided in Table 2. The uncertainty associated with growth temperature relates to an uncertainty of the position of the origin in Figure S2. For a given sample, total uncertainty arising from analytical uncertainty and from potential seasonal bias in growth temperature can be easily displayed propagating these two sources of uncertainties. For this purpose, differences between mean annual and seasonal maximum and minimum temperature (Table 3), respectively, were converted to uncertainties $d\Delta_{i,\,pred.,\,lower}$ and $d\Delta_{i,\,pred.,\,upper}$ considering that the mean annual temperature for a given location often does not represent the average of minimum and maximum seasonal temperatures:

$d\Delta_{i,\,pred.,\,lower}$ = (Δ_i, pred. for lowest habitat T) – (Δ_i, pred. for mean annual habitat T) (A.1)

$d\Delta_{i,\,pred.,\,upper}$ = (Δ_i, pred. for highest habitat T) – (Δ_i, pred. for mean annual habitat T) (A.2)

Total uncertainties were then calculated for lower and upper boundary levels separately applying Gaussian error propagation:

$$d\Delta_{i,total,\,upper.} = \sqrt{(d\Delta_{i,pred.,lower})^2 + (d\Delta_i)^2} \quad (A.3)$$

$$d\Delta_{i,total,\,lower.} = \sqrt{(d\Delta_{i,pred.,upper})^2 + (d\Delta_i)^2} \quad (A.4)$$

where $\Delta_{i,total,\ upper}$ and $\Delta_{i,total,\ lower}$ represent the upper and lower boundary levels of total Δ_i uncertainties, respectively. Samples that exhibit Δ_{47} and Δ_{48} values consistent with those predicted by the monitored seasonal temperature range should plot within their $d\Delta_{i,total,\ upper}$ or $d\Delta_{i,total,\ lower}$ boundary levels indistinguishable from the origin. With the exception of RG2, this is the case for all investigated modern specimen.

Results of the applied bootstrapping approach (see Section 3.2) are shown in Supplementary Figure S3.

Compiled oxygen isotope data on molluscs and seawater and corresponding habitat temperatures are available in Supplementary Table S1. Baseline-corrected clumped isotope input data (δ^{45}-δ^{49}) as well as Δ_{47}, Δ_{48}, $\delta^{18}O$, and $\delta^{13}C$ results can be found in Supplementary Tables S2 (pooled over all RG2 aliquots) and S3 (RG2 and RG2_U aliquots evaluated separately), along with processing statistics.

Data Availability

All data is accessible from https://doi.org/10.5281/zenodo.14961836.

References

Arndt, I., Bernecker, M., Erhardt, T., Evans, D., Fiebig, J., Fursman, M., Kniest, J., Renema, W., Schlidt, V., Staudigel, P., Voigt, S., Müller, W., 2024. 20,000 days in the life of a giant clam reveal late Miocene tropical climate variability. Palaeogeography, Palaeoclimatology, Palaeoecology 661, 112711

Addadi, L., Raz, S., Weiner, S., 2003. Taking advantage of disorder: amorphous calcium carbonate and its roles in biomineralization. Advanced Materials 15, 959-970

Addadi, L., Joester, D., Nudelman, F., Weiner, S., 2006. Mollusk shell formation: A source of new concepte for understanding biomineralization process. Chemistry A European Journal 12, 980-987

Adkins, J. F., Boyle, E. A., Curry, W. B., Lutringer, A., 2003. Stable isotopes in deep-sea corals and a new mechanism for "vital effects". Geochimica et Cosmochimica Acta 67, 1129-1143

Affek, H. P., 2013. Clumped isotopic equilibrium and the rate of isotope exchange between CO_2 and water. American Journal of Science 313, 309-325

Affek, H. P., Matthews, A., Ayalon, A., Bar-Matthews, M., Burstyn, Y., Zaarur, S., Zilberman, T., 2014. Accounting for kinetic isotope effects in Soreq Cave (Israel) speleothems. Geochimica et Cosmochimica Acta 143, 303-318

Affek, H. P., Zaarur, S., 2014. Kinetic isotope effect in CO_2 degassing: Insight from clumped and oxygen isotopes in laboratory precipitation experiments. Geochimica et Cosmochimica Acta 143, 319-330

Anderson, N. T., Kelson, J. R., Kele, S., Daëron, M., Bonifacie, M., Horita, J., Mackey T. J., John, C. M., Kluge, T., Petschnig, P., Jost, A. B., Huntington, K. W., Bernasconi, S. M., Bergmann, K. D., 2021. A Unified Clumped Isotope Thermometer Calibration (0.5-1,100°C) Using Carbonate-Based Standardization. Geophysical Research Letters 48:7, e2020GL092069

Bajnai, D., Fiebig, J., Tomasovych, A., Milner Garcia, S., Rollion-Bard, C., Raddatz, J., Löffler, N., Primo-Ramos, C., Brand, U., 2018. Assessing kinetic fractionation in brachiopod calcite using clumped isotopes. Scientific Reports 8:533 (DOI:10.1038/s41598-017-17353-7)

Bajnai, D., Guo, W., Löffler, N., Methner, K., Krsnik, E., Coplen, T. B., Gischler, E., Hansen, M., Henkel, D., Price, G. D., Raddatz, J., Scholz, D., Fiebig, J., 2020. Combined clumped isotope measurements resolve kinetic biases in carbonate formation temperatures. Nature Communications 11:4005

Batenburg, S. J., Reichart, G.-J., Jilbert, T., Janse, M., Wesselingh, F. P., Renema, W., 2011. Interannual climate variability in the Miocene: High resolution trace element and stable isotope ratios in giant clams. Palaeogeography, Palaeoclimatology, Palaeoecology 306, 75-81

Bernasconi, S. M., Müller, I. A., Bergmann, K. D., Breitenbach, S. F. M., Fernandez, A., Hodell, D. A., Jaggi, M., Meckler, A. N., Millan, I., Ziegler, M., 2018. Reducing uncertainties

812 in carbonate clumped isotope analysis through consistent carbonate-based standardization.
813 Geochemistry, Geophysics, Geosystems 19:9, 2895-2914

814 Bernecker, M., Hofmann, S., Staudigel, P.T., Davies, A.J., Tagliavento, M., Meijer, N., Ballian,
815 A., Fiebig, J., 2023. A robust methodology for triple (Δ_{47}, Δ_{48}, Δ_{49}) clumped isotope analysis of
816 carbonates. Chemical Geology 642, 121803

817 Bernecker, M., Bonifacie, M., Staudigel, P., Meijer, N., Siebert, J., Wehr, N., Haussühl, E.,
818 Bernasconi, S.M., Petrash, D.A., Dietzel, M., Fiebig, J., 2025. Effects of mineralogy on Δ_{47} and
819 Δ_{48} of carbonate-derived CO_2 below analytical resolution. Geochimica et Cosmochimica Acta
820 401, 89-103

821 Bertucci, A., Moya, A., Tambutté, S., Allemand, D., Supuran, C. T., Zoccola, D., 2013.
822 Carbonic anhydrases in anthozoan corals – A review. Bioorganic & Medical Chemistry 21,
823 1437-1450

824 Bijl, P. K., Schouten, S., Sluijs, A., Reichart, G.-J., Zachos, J. C., Brinkhuis, H., 2009. Early
825 Palaeogene temperature evolution of the southwest Pacific Ocean. Nature 461, 776-779

826 Burnett, L. E., 1988. Physiological responses to air exposure: acid-base balance and the role of
827 branchial water stores. Amer. Zool. 28, 125-135

828 Butler, P. G., Wanamaker, A. D., Scourse, J. D., Richardson, C. A., and Reynolds, D. J., 2013.
829 Variability of marine climate on the North Icelandic Shelf in a 1357-year proxy archive based
830 on growth increments in the bivalve Arctica islandica. Palaeogeography, Palaeoclimatology,
831 Palaeoecology, 373, 141–151

832 Caldarescu, D. E., Sadatzki, H., Andersson, C., Schäfer, P., Fortunato, H., Meckler, A. N., 2021.
833 Clumped isotope thermometry in bivalve shells: A tool for reconstructing seasonal upwelling.
834 Geochimica et Cosmochimica Acta 294, 174-191

835 Cardoso, J. C. R., Ferreira, V., Zhang, X., Anjos, L., Félix, R. C., Batista, F. M., Power, D. M.,
836 2019. Evolution and diversity of alpha-carbonic anhydrases in the mantle of the Mediterranean
837 mussel (Mytilus galloprovincialis). Scientific Reports 9, 10400

838 Carré, M., Bentaleb, I., Bruguier, O., Ordinola, E., Barrett, N. T., Fontugne, M., 2006.
839 Calcification rate influence on trace element concentrations in aragonitic bivalve shells:
840 Evidences and mechanisms. Geochimica et Cosmochimica Acta 70, 4906-4920

841 Chen, S., Gagnon, A. C., Adkins, J. F., 2018. Carbonic anhydrase, coral calcification and a new
842 model of stable isotope vital effects. Geochimica et Cosmochimica Acta 236, 179-197

843 Clark, A. J., Vellekoop, J., Speijer, R. P., 2022. Hydrological differences between the Lutetian
844 Paris and Hampshire basins revealed by stable isotopes of conid gastropods, Bulletin de la
845 Société Géologique de France, 193, 3

846 Coplen, T. B., 2007. Calibration of the calcite-water oxygen-isotope geothermometer at Devils
847 Hole, Nevada, a natural laboratory. Geochimica et Cosmochimica Acta 71, 3948-3957

Crenshaw, M. A., 1972. The soluble matrix of Mercenaria mercenaria shell. Biomineralization 6, 6-11

Curley A. N., Petersen S. V., Stewart M. E., Guo W. 2023. Biologically driven isotopic fractionations in bivalves: from paleoenvironmental problem to palaeophysiological proxy. Biological Reviews 98, 1016-1032

Daëron, M., Guo, W., Eiler, J., Genty, D., Blamart, D., Boch, R., Drysdale, R., Maire, R., Wainer, K., Zanchetta, G., 2011. $^{13}C^{18}O$ clumping in speleothems: Observations from natural caves and precipitation experiments. Geochimica et Cosmochimica Acta 75, 3303-3317

Daëron, M., Drysdale, R. N., Peral, M., Hyughe, D., Blamart, D., Coplen, T. B., Lartaud, F., Zanchetta, G., 2019. Most Earth-surface calcites precipitate out of isotopic equilibrium. Nature Communications 10:429

Daëron, M., 2021. Full Propagation of Analytical Uncertainties in Δ_{47} Measurements. Geochemistry, Geophysics, Geosystems 22:5

Davies, A. J., John, C. M., 2019. The clumped (^{13}C-^{18}O) isotope composition of echinoid calcite: Further evidence for "vital effects" in the clumped isotope proxy. Geochimica et Cosmochimica Acta 245, 172-189

Davies, A. J., Davis, S., John, C. M., 2021. Evidence of taxonomic non-equilibrium effects in the clumped isotope composition of modern cephalopod carbonate. Chemical Geology 578, 120317

Davies, A. J., Guo, W., Bernecker, M., Tagliavento, M., Raddatz, J., Gischler, E., Flögel, S., Fiebig, J., 2022. Dual clumped isotope thermometry of coral carbonate. Geochimica et Cosmochimica Acta 338, 66-78

Davies, A. J., Brand, U., Tagliavento, M., Bitner, M. A., Bajnai, D., Staudigel, P. T., Bernecker, M., Fiebig, J., 2023. Isotopic disequilibrium in brachiopods disentangled with dual clumped isotope thermometry. Geochimica et Cosmochimica Acta 359, 135-147

Defliese, W. F., Hren, M. T., Lohmann, K. C., 2015. Compositional and temperature effects of phosphoric acid fractionation on Δ_{47} analysis and implications for discrepant calibrations. Chemical Geology 396, 51-60

De Man, E., Ivany, L., Vandenberghe, N., 2004. Stable oxygen isotope record of the Eocene-Oligocene transition in the southern North Sea Basin: positioning the Oi-1 event. Netherlands. Journal of Geosciences / Geologie en Mijnbouw 83, 193-197

Dennis, K. J., Affek, H. P., Passey, B. H., Schrag, D. P., Eiler, J. M., 2011. Defining an absolute reference frame for 'clumped' isotope studies of CO_2. Geochimica et Cosmochimica Acta 75, 7117-7131

de Winter, N. J., Vellekoop, J., Clark, A. J., Stassen, P., Speijer, R., Claeys, P., 2020. The giant marine gastropod Campanile giganteum (Lamarck, 1804) as a high-resolution archive of

seasonality in the Eocene greenhouse world. Geochemistry, Geophysics, Geosystems 21:4, e2019GC008794

de Winter, N. J., Dämmer, L. K., Falkenroth, M., Reichart, G.-J., Moretti, S., Martínez-García, A., Höche, N., Schöne, B. R., Rodiouchkina, K., Goderis, S., Vanhaecke, F., van Leeuwen, S. M., and Ziegler, M., 2021a. Multi-isotopic and trace element evidence against different formation pathways for oyster microstructures, Geochimica et Cosmochimica Acta, 308, 326–352, https://doi.org/10.1016/j.gca.2021.06.012

de Winter, N. J., Agterhuis, T., Ziegler, M., 2021b.: Optimizing sampling strategies in high-resolution paleoclimate records, Climate of the Past 17, 1315–1340.

de Winter, N. J., Witbaard, R., Kocken, I. J., Müller, I. A., Guo, J., Goudsmit, B., Ziegler, M., 2022. Temperature dependence of clumped isotopes (Δ_{47}) in aragonite. Geophysical Research Letters 49, e2022GL099479

Dietzel, M., Tang, J., Leis, A., Köhler S. J., 2009. Oxygen isotopic fractionation during inorganic calcite precipitation – effects of temperature, precipitation rate and pH. Chemical Geology 268, 107-115

Evans, D., Sagoo, N., Renema, W., Cotton, L. J., Müller, W., Todd, J. A., Saraswati, P. K., Stassen, P., Ziegler, M., Pearson, P. N., Valdes, P. J., Affek, H. P., 2018. Eocene greenhouse climate revealed by coupled clumped isotope-Mg/Ca thermometry. Proceedings of the National Academy of Sciences USA 115, 1174-1179.

Fiebig, J., Bajnai, D., Löffler, N., Methner, K., Krsnik, E., Mulch, A., Hofmann, S., 2019. Combined high-precision Δ_{48} and Δ_{47} analysis of carbonate. Chemical Geology 522, 186-191

Fiebig, J., Daeron, M., Bernecker, M., Guo, W., Schneider, G., Boch, R., Bernasconi, S. M., Jautzy, J., Dietzel, M., 2021. Calibration of the dual clumped isotope thermometer for carbonates. Geochimica et Cosmochimica Acta 312, 235-256

Fiebig, J., Bernecker, M., Meijer, N., Methner, K., Staudigel, P. T., Davies, A. J., Bayarjargal, L., Spahr, D., Winkler, B., Hofmann, S., Granzin, M., Petersen, S. V., 2024. Carbonate clumped isotope values compromised by nitrate-derived NO_2 interferent. Chemical Geology 670: 122382

Fitzer, S. C., Chung, P., Maccherozzi, F., Dhesi, S. S., Kamensos, N. A., Phoenix, V. R., Cusack, M., 2016. Biomineral shell formation under ocean acidification: a shift from order to chaos. Scientific Reports 6, 21076

Freeman, J. A., Willbur, K. M., 1948. Carbonic anhydrase in molluscs. The Biological Bulletin 94, 55-59

Ghosh, P., Adkins, J., Affek, H., Balta, B., Guo, W., Schauble, E. A., Schrag, D., Eiler, J. M., 2006. ^{13}C-^{18}O bonds in carbonate minerals: A new kind of paleothermometer. Geochimica et Cosmochimica Acta 70, 1439-1456

Goodwin, D. H., Flessa, K. W., Schöne, B. R., and Dettman, D. L.: Cross-calibration of daily growth increments, stable isotope variation, and temperature in the Gulf of California bivalve

mollusk Chione cortezi: implications for paleoenvironmental analysis, Palaios, 16, 387–398, 2001.

Grossman, E. L., Ku, T.-L., 1986. Oxygen and carbon isotope fractionation in biogenic aragonite: temperature effects. Chemical Geology 59, 59-74

Guo, W., 2020. Kinetic clumped isotope fractionation in the DIC-H_2O-CO_2 system: Patterns, controls, and implications. Geochimica et Cosmochimica Acta 268, 230-257

Guo, W., Zhou, C., 2019. Patterns and controls of disequilibrium isotope effects in speleothems: Insights from an isotope-enabled diffusion-reaction model and implications for quantitative thermometry. Geochimica et Cosmochimica Acta 267, 196-226

Harwood, A. J. P., Dennis, P. F., Marca, A. D., Pilling, G. M., Millner, R. S., 2008. The oxygen isotope composition of water masses within the North Sea. Estuarine, Coastal and Shelf Science 78, 353-359

Henkes, G. A., Passey, B. H., Wanamaker Jr., A. D., Grossman, E. L., Ambrose Jr., W. G., Carroll, M. L., 2013. Carbonate clumped isotope compositions of modern marine mollusc and brachiopod shells. Geochimica et Cosmochimica Acta 106, 307-325

Hill, P. S., Tripati, A. K., Schauble, E. A., 2014. Theoretical constraints on the effects of pH, salinity, and temperature on clumped isotope signatures of dissolved inorganic carbon species and precipitating carbonate minerals. Geochimica et Cosmochimica Acta 125, 610-651

Huyghe, D., Lartaud, F., Emmanuel, L., Merle, D., and Renard, M.: Palaeogene climate evolution in the Paris Basin from oxygen stable isotope ($\delta^{18}O$) compositions of marine molluscs, Journal of the Geological Society, 172, 576–587, 2015.

Huyghe, D., Daeron, M., de Rafelis, M., Blamart, D., Sébilo, M., Paulet, Y.-M., Lartaud, F., 2022. Clumped isotopes in modern marine bivalves. Geochimica et Cosmochimica Acta 316, 41-58

Immenhauser, A., Schöne, B. R., Hoffmann, R., Niedermayr, A., 2016. Mollusc and brachiopod skeletal hard parts: Intricate archives of their marine environment. Sedimentology 63, 1-59

Ingalls, M., Leapaldt, H.C., Lloyd, M.K., 2024. Microbial autotrophy recorded by carbonate dual clumped isotope disequilibrium. Geochemistry, Geophysics, Geosystems 25, e2024GC011590.

Inglis, G. N., Farnsworth, A., Lunt, D., Foster, G. L., Hollis, C. J., Pagani, M., Jardine, P. E., Pearson, P. N., Markwick, P., Galsworthy, A. M. J., Raynham, L., Taylor, K. W. R., Pancost, R. D., 2015. Descent toward the Icehouse: Eocene sea surface cooling inferred from GDGT distributions. Paleoceanography 30, 1000-1020

Inglis, G. M, Bhatia, R., Evans, D., Zhu, J., Müller, W., Mattey, D., Thornalley, D. J. R., Stockey, R. G., Wade, B. S., 2023. Surface ocean cooling in the Eocene North Atlantic coincides with declining atmospheric CO_2. Geophysical Research Letters 50:24, e2023GL105448

Ip, Y. K., Loong, A. M., Hiong, K. C., Wong, W. P., Chew, S. F., Reddy, K., Sivaloganathan, B., Ballantyne, J. S., 2006. Light induces an increase in the pH of and a decrease in the ammonia concentration in the extrapallial fluid of the giant clam Tridacna squamosa. Physiological and Biochemical Zoology 79, 656-664

Ivany, L.C., Judd, E.J., 2022. Deciphering Temperature Seasonality in Earth's Ancient Oceans. Annual Review of Earth and Planetary Sciences, 50, 123–152.

Jacob, D. E., Wirth, R., Soldati, A. L., Wehrmeister, U., Schreiber, A. 2011. Amorphous calcium carbonate in the shells of adult *Unionoida*. Journal of Structural Biology 173:2, 241-249

Janse, M., Wensing, J., Gieling, H., de Jongh, T., Leewis, R., 2008. Ecological management of a large coral reef eco-display at Burgers' Zoo, Arnhem, The Netherlands. *Advances in Coral Husbandry in Public Aquariums Public Aquarium Husbandry Series, eds RJ Leewis and M. Janse (Arnhem: Burgers' Zoo)*, pp.293-303.

Jansen, J. M., Pronker, A. E., Kube, S., Sokolowski, A., Sola, J. C., Marquiegui, M. A., Schiedek, D., Bonga, S. W., Wolowicz, M., Hummel, H., 2007. Geographic and seasonal patterns and limits on the adaptive response to temperature of European *Mytilus* spp. and *Macoma balthica* populations. Oecologia 154, 23-34

Jautzy, J., Savard, M., Dhillon, R., Bernasconi, S., Lavoie, D., Smirnoff, A., 2020. Clumped isotope temperature calibration for calcite: Bridging theory and experimentation. Geochemical Perspective Letters 14, 36-41

Judd, E. J., Wilkinson, B. H., and Ivany, L. C., 2017. The life and time of clams: Derivation of intra-annual growth rates from high-resolution oxygen isotope profiles. Palaeogeography, Palaeoclimatology, Palaeoecology 490, 70-83

Judd, E. J., Tierney, J. E., Lunt, D. J., Montañez, I. P., Huber, B. T., Wing, S. L., and Valdes, P. J., 2024. A 485-million-year history of Earth's surface temperature. Science 385, eadk3705

Kaandorp, R. J. G., Vonhof, H. B., Del Busto, C., Wesselingh, F. P., Ganssen, G. M., Marmól, A. E., Romero Pittman, L., and van Hinte, J. E., 2003. Seasonal stable isotope variations of the modern Amazonian freshwater bivalve *Anodontites trapesialis*. Palaeogeography, Palaeoclimatology, Palaeoecology 194, 339–354

Kelson, J. R., Huntington, K. W., Schauer, A. J., Saenger, C., Lechler, A. R., 2017. Toward a universal carbonate clumped isotope calibration: Diverse synthesis and preparatory methods suggest a single temperature relationship. Geochimica et Cosmochimica Acta 197, 104-131

Kim, S.-T., O'Neil, J. R., 1997. Equilibrium and nonequilibrium oxygen isotope effects in synthetic carbonates. Geochimica et Cosmochimica Acta 61, 3461-3475

Kim, S.-T., Mucci, A., Taylor, B. E., 2007a. Phosphoric acid fractionation factors for calcite and aragonite between 25 and 75°C: Revisited. Chemical Geology 246, 135-146

996 Kim, S.-T., O'Neil, J. R., Hillaire-Marcel, C., Mucci, A., 2007b. Oxygen isotope fractionation
997 between synthetic aragonite and water: Influence of temperature and Mg^{2+} concentration.
998 Geochimica et Cosmochimica Acta 71, 4704-4715

999 Kniest, J. F., Davies, A. J., Brugger, J., Fiebig, J., Bernecker, M., Todd, J. A., Hickler, T., Voigt,
1000 S., Woodland, A., Raddatz, J., 2024a. Dual clumped isotopes from the Mid-Eocene bivalve
1001 shell reveal a hot and summer wet climate of the Paris Basin. Communications Earth &
1002 Environment 5: 330

1003 Kniest, J. F., Evans, D., Gerdes, A., Cantine, M., Todd, J. A., Sigwart, J. D., Vellekoop, J.,
1004 Müller, W., Voigt, S., Raddatz, J., 2024b. Spatiotemporal changes in riverine input into the
1005 Eocene North Sea revealed by strontium isotope and barium analysis of bivalve shells.
1006 Scientific Reports 14: 28806

1007 Lécuyer, C., Hutzler, A., Amiot, R., Daux, V., Grosheny, D., Otero, O., Martineau, F., Fourel,
1008 F., Balter, V., Reynard, B., 2012. Carbon and oxygen isotope fractionations between aragonite
1009 and calcite of shells from modern molluscs. Chemical Geology 332-333, 92-101

1010 Lécuyer, C., Reynard, B., Martineau, F., 2004. Stable isotope fractionation between mollusc
1011 shells and marine waters from Martinique Island. Chemical Geology 213, 293-305

1012 Le Roy, N., Jackson, D. J., Marie, B., Ramos-Silva, P., Marin, F., 2016. Carbonic anhydrase
1013 and metazoan biocalcification: A focus on molluscs. Key Engineering Materials 672, 151.157

1014 Levitt, N., P., Eiler, J. M., Romanek, C. S., Beard, B. L., Xu, H., Johnson, C. M., 2018. Near
1015 equilibrium ^{13}C-^{18}-O bonding during inorganic calcite precipitation under chemo-stat
1016 conditions. Geochemistry, Geophysics, Geosystems 19, 901-920

1017 Levitus, S., Boyer, T.P, Garcia, H.E., Locarnini, R.A., Zweng, M.M., Mishonov, A.V., Reagan,
1018 J.R., Antonov, J.I., Baranova, O.K., Biddle, M., Hamilton, M., Johnson, D.R., Paver, C.R.,
1019 Seidov, D. (2015). World Ocean Atlas 2013 (NCEI Accession 0114815). [Temperature
1020 dataset]. NOAA National Centers for Environmental Information.
1021 Dataset. https://doi.org/10.7289/v5f769gt

1022 Lindinger, M. I., Lauren, D. J., McDonald, D. G., 1984. Acid-base-balance in the sea mussel,
1023 Mytilus edulis. 3. Effects of environmental hypercapnia on intracellular and extracellular acid-
1024 base-balance. Marine Biology Letters 5, 371-381

1025 Locarnini, R.A., A.V. Mishonov, O.K. Baranova, J.R. Reagan, T.P. Boyer, D. Seidov, Z. Wang,
1026 H.E. Garcia, C. Bouchard, S.L. Cross, C.R. Paver, and D. Dukhovskoy (2024). World Ocean
1027 Atlas 2023, Volume 1: Temperature. A. Mishonov Technical Editor, NOAA Atlas NESDIS 89,
1028 doi.org/10.25923/54bh-1613.

1029 Lu, C., Murray, S.T., Klaus, J., McNeill, D.F., Swart, P.K. (2024) Dual clumped isotopes ((Δ_{47}
1030 and Δ_{48}) reveal non-equilibrium formation of freshwater cements. Geochimica et
1031 Cosmochimica Acta 379, 145-157.

1032 Lu, C.L., Swart, P.K., (2024) The application of dual clumped isotope thermometer ((Δ_{47} and
1033 Δ_{48}) to the understanding of dolomite formation. Geology 52, 56-60.

Marchegiano, M., John, C. M., 2022. Disentangling the impact of global and regional climate changes during the Middle Eocene in the Hampshire Basin: New insights from carbonate clumped isotopes and ostracod assemblages. Paleoceanography and Paleoclimatology 37, e2021PA004299

Marie, B., Luquet, G., Bédouet, L., Milet, C., Guichard, N., Medakovic, D., Marin, F., 2008. Nacre Calcification in the Freshwater Mussel *Unio pictorium*: Carbonic Anhydrase Activity and Purificaion of a 95 kDa Calcium-Binding Glycoprotein. ChemBioChem 9, 2515-2523

McConnaughey, T., 1989a. ^{13}C and ^{18}O disequilibrium in biological carbonates: I. Patterns. Geochimica et Cosmochimica Acta 53, 151-162

McConnaughey, T., 1989b. ^{13}C and ^{18}O isotopic disequilibrium in biological carbonates: II. *In vitro* simulation of kinetic isotope effects. Geochimica et Cosmochimica Acta 53, 163-171

Miyamoto, H., Miyashita, T., Okushima, M., Nakano, S., Morita, T., Matsushiro, A., 1996. A carbonic anhydrase from the nacreous layer in oyster pearls. Proceedings of the National Academy of Sciences USA 93, 9657-9660

Miyamoto, H., Miyoshi, F., Kohno, J., 2005. The carbonic anhydrase domain protein nacrein is expressed in the epithelial cells of the mantle and acts as a negative regulator in calcification in the mollusk Pinctada fucata. Zoological Science 22, 311-315

Nassif, N., Pinna, N., Gehrke, N., Antonietti, M., Jäger, C., Cölfen H., 2005. Amorphous layer around aragonite platelets in nacre. Proceedings of the National Academy of Sciences USA 102, 36, 12653-12655

Nehrke, G., Poigner, H., Wilhelms-Dick, D., Brey, T., Abele, D., 2012. Coexistencew of three calcium carbonate polymorphs in the shell of the Antarctic clam Laternula elliptica. Geochemistry, Geophysics, Geosystems 13:5

Nielsen, S. A., Frieden, E., 1972. Carbonic anhydrase activity in molluscs. Comparative Biochemistry and Physiology 41B, 461-468

Nooitgedacht, C. W., van der Lubbe, H. J. L., Ziegler, M., Staudigel, P. T., 2021. Internal water facilitates thermal resetting of clumped isotopes in biogenic aragonite. Geochemistry, Geophysics, Geosystems 22, e2021GC009730

Park, D.-K., Lee, M. S., 2019. Kinetic study of catalytic CO_2 hydration by metal-substituted biomimetic carbonic anhydrase model complexes. Royal Society Open Science 6:190407.

Parvez, Z.A., Lucarelli, J.K., Matamaros, I.W., Rubi, J., Miguel, K., Elliott, B., Flores, R., Ulrich, R.N., Eagle, R.A., Watkins, J.M., Christensen, J.N., Tripati, A., 2023. Dual carbonate clumped isotopes (Δ_{47}-Δ_{48}) constrains kinetic effects and timescales in peridotite-associated springs at the Cedars, Northern California. Geochimica et Cosmochimica Acta 358, 77-92.

Parvez, Z.A., El-Shenawy, M., Lucarelli, J.K., Kim, S.T., Johnson, K.R., Wright, K., Gebregiorgis, D., Montanez, I.P., Wortham, B., Asrat, A., Reinhardt, E., Christensen, J.N., Matamoros, I.W., Rubi, J., Miguel, K., Elliott, B.M., Flores, R., Kovacs, S., Eagle, R.A., Tripati,

A., 2024. Dual carbonate clumped isotope ((Δ_{47}-Δ_{48}) measurements constrain different sources of kinetic isotope effects and quasi-equilibrium signatures in cave carbonates. Geochimica et Cosmochimica Acta 366, 95-112.

Payne, J.L., Heim, N.A., Knope, M.L., McClain, C.R., 2014. Metabolic dominance of bivalves predates brachiopod diversity decline by more than 150 million years. Proceedings of the Royal Society B 281, 20133122.

Pederson, C., Mavromatis, V., Dietzel, M., Rollion-Bard, C., Nehrke, G., Jöns, N., Jochum, K. P., Immenhauser, A., 2019. Diagenesis of mollusc aragonite and the role of fluid reservoirs. Earth and Planetary Science Letters 514, 130-142

Ross, C. L., Warnes, A., Comeau, S., Cornwall, C. E., Cuttler, M. V. W., Naugle, M., McCulloch, M. T., Schoepf, V., 2022. Coral calcification mechanisms in a warming ocean and the interactive effects of temperature and light. Communications Earth and Environment 3:72

Sade, Z., Halevy, I., 2017. New constraints on kinetic isotope effects during CO_2(aq) hydration and hydroxylation: Revisiting theoretical and experimental data. Geochimica et Cosmochimica 214, 246-265

Saenger, C., Affek, H. P., Felis, T., Thiagarajan, N., Lough, J. M., Holcomb, M., 2012. Carbonate clumped isotope variability in shallow water corals: Temperature dependence and growth-related vital effects. Geochimica et Cosmochimica Acta 99, 224-242

Saenger, C., Gabitov, R. I., Farmer, J., Watkins, J. M., Stone, R., 2017. Linear correlations in bamboo coral $\delta^{13}C$ and $\delta^{18}O$ sampled by SIMS and micromill: Evaluating paleoceanographic potential and biomineralization mechanisms using $\delta^{11}B$ and Δ_{47} composition. Chemical Geology 454, 1-14

Schauble, E.A., Ghosh, P., Eiler, J.M., 2006. Preferential formation of ^{13}C-^{18}O bonds in carbonate minerals, estimated using first-principles lattice dynamics. Geochimica et Cosmochimica Acta 70, 2510-2529

Schmidt, G.A., G. R. Bigg and E. J. Rohling. 1999. "Global Seawater Oxygen-18 Database - v1.22" https://data.giss.nasa.gov/o18data/

Schöne, B. R., Fiebig, J., Pfeiffer, M., Gleβ, R., Hickson, J., Johnson, A. L., Dreyer, W., Oschmann, W., 2005. Climate records from a bivalved Methuselah (*Arctica islandica*, Mollusca; Iceland), Palaeogeography, Palaeoclimatology, Palaeoecology, 228, 130–148

Spooner, P. T., Guo, W., Robinson, L. F., Thiagarajan, N., Hendry, K. R., Rosenheim, B. E., Leng, M. J., 2016. Clumped isotope composition of cold-water corals: A role for vital effects? Geochimica et Cosmochimica Acta 179, 123-141

Staudigel, P. T., Pederson, C., van der Lubbe, J., Bernecker, M., Tagliavento, M., Davies, A. J., Immenhauser, A., Fiebig, J. (2023a). An isotopologue-enabled model (Δ_{47}, Δ_{48}) for describing thermal fluid-carbonate interaction in open and closed diagenetic systems. Geochemistry, Geophysics, Geosystems 24, e2023GC011117.

Staudigel, P., Davies, A.J., Bernecker, M., Tagliavento, M., van der Lubbe, H.J.L., Nooitgedacht, C., Looser, N., Bernasconi, S.M., Vonhof, H., Price, G., Fiebig, J. (2023b) Fingerprinting kinetic isotope effects and diagenetic exchange reactions using fluid inclusion and dual-clumped isotope analysis. Geochemistry, Geophysics, Geosystems 24, e2022GC010766.

Staudigel, P. T., Feng, D., Peckmann, J., Bernecker, M., Davies, A. J., Tagliavento, M., Fiebig, J., 2024. Resolving and correcting for kinetic biases on methane seep paleotemperature using carbonate Δ_{47}/Δ_{48} analysis. Science Advances 10, eadn0155.

Swart, P.K., Lu, C., Moore, E.W., Smith, M.E., Murray, S.T., Staudigel, P.T. (2021) A calibration equation between Δ_{48} values of carbonate and temperature. Rap. Commun. Mass Spectrom. 35, e9147.

Tagliarolo, M., Grall, J., Chavaud, L., Clavier, J., 2013a. Aerial and underwater metabolism of Patella vulgata L.: comparison of three intertidal levels. Hydrobiologia 702, 241-253

Tagliarolo, M., Clavier, J., Chauvaud, L., Grall, J., 2013b. Carbon emission associated with respiration and calcification of nine gastropod species from the intertidal rocky shore of Western Europe. Marine Biology 160, 2891-2901

Tagliavento, M., Davies, A. J., Bernecker, M., Staudigel, P. T., Dawson, R. R., Dietzel, M., Götschl, K., Guo, W., Schulp, A. S., Therrien, F., Zelenitsky, D. K., Gerdes, A., Müller, W., Fiebig, J., 2023. Evidence for heterothermic endothermy and reptile-like eggshell mineralization in Troodon, a non-avian maniraptoran theropod. Proceedings of the National Academy of Sciences USA 120, e2213987120

Thiagarajan, N., Adkins, J., Eiler, J., 2011. Carbonate clumped isotope thermometry of deep-sea corals and implications for vital effects. Geochimica et Cosmochimica Acta 75, 4416-4425

Tripati, A. K., Hill, P. S., Eagle, R. A., Mosenfelder, J. L., Tang, J., Schauble, E. A., Eiler, J. M., Zeebe, R. E., Uchikawa, J., Coplen, T. B., Ries, J. B., Henry, D., 2015. Beyond temperature: Clumped isotope signatures in dissolved inorganic carbon species and the influence of solution chemistry on carbonate mineral composition. Geochimica et Cosmochimica Acta 166, 344-371

Uchikawa, J., Zeebe, R. E., 2012. The effect of carbonic anhydrase on the kinetics and equilibrium of the oxygen isotope exchange in the CO_2-H_2O system: Implications for $\delta^{18}O$ vital effects in biogenic carbonates. Geochimica et Cosmochimica Acta 95, 15-34

Venn, A. A., Tambutté, E., Caminti-Segonds, N., Techer, N., Allemand, D., Tambutté, S., 2019. Effects of light and darkness on pH ragulation in three coral species exposed to seawater acidification. Scientific Reports 9:2201

Vihtakari, M., Renaud, P. E., Clarke, L. J., Whitehouse, M. J., Hop, H., Carroll, M. L., Ambrose Jr, W. G., 2016. Decoding the oxygen isotope signal for seasonal growth patterns in Arctic bivalves. Palaeogeography, Palaeoclimatology, Palaeoecology 446, 263-283

Wang, Z., Gaetani, G., Liu, C., Cohen, A., 2013. Oxygen isotope fractionation between aragonite and seawater: Developing a novel kinetic oxygen isotope fractionation model. Geochimica et Cosmochimica Acta 117, 232-251

Watkins, J.M., Nielsen, L.C., Ryerson, F.J., Paolo, D.J., 2013. The influence of kinetics on the oxygen isotope composition of calcium carbonate. Earth and Planetary Science Letters 375, 349-360

Watkins, J.M., Hunt, J.D., Ryerson, F.J., Paolo, D.J., 2014. The influence of temperature, pH, and growth rate on the $\delta^{18}O$ composition of inorganically precipitated calcite. Earth and Planetary Science Letters 404, 332-343

Weber, J.N., Woodhead P.M.J., 1972. Temperature dependence of oxygen-18 concentration in reef coral carbonates. Journal of Geophysical Research 77, 463–473

Weiss I. M., Tuross N., Addadi L., Weiner S., 2002. Mollusc Larval Shell Formation: Amorphous Calcium Carbonate is a Precursor Phase for Aragonite. Journal of Experimental Zoology 293, 478–491

White, J. H., Defliese, W. F., 2023. $\delta^{13}C$ and $\delta^{18}O$ heterogeneities in carbonates: Nonlinear mixing in the application of dual-carbonate-clumped isotope thermometer. Rapid Communications in Mass Spectrometry 37, e9627

Witbaard, R., Jenness, M. I., Van Der Borg, K., and Ganssen, G., 1994. Verification of annual growth increments in Arctica islandica L. from the North Sea by means of oxygen and carbon isotopes. Netherlands Journal of Sea Research, 33, 91–101

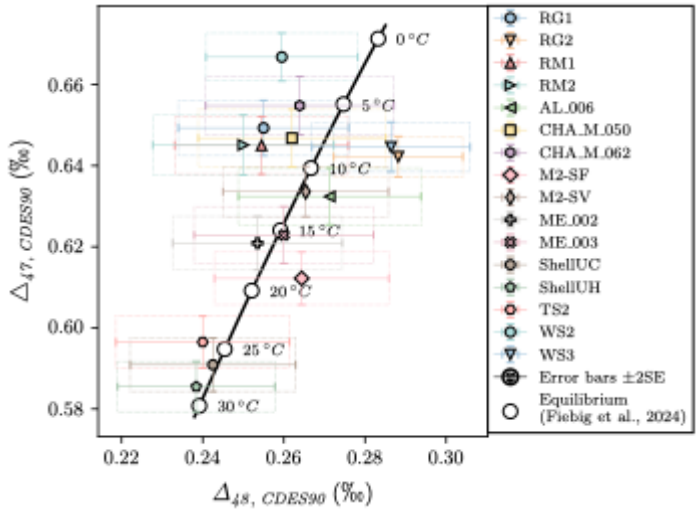

Fig. 1. Dual clumped isotope composition of modern molluscs.

Δ_{47}/Δ_{48} values of all modern samples are shown relative to the position of equilibrium (Fiebig et al., 2024). Error bars represent fully propagated 2SE measurement uncertainties.

Commented [DE26]: Note that this appears heavily pixellated on my screen - please export at a higher resolution, ideally as a vector file.

Why does 'error bars +2SE appear in the legend? It can be deleted there since you specify this in the caption.

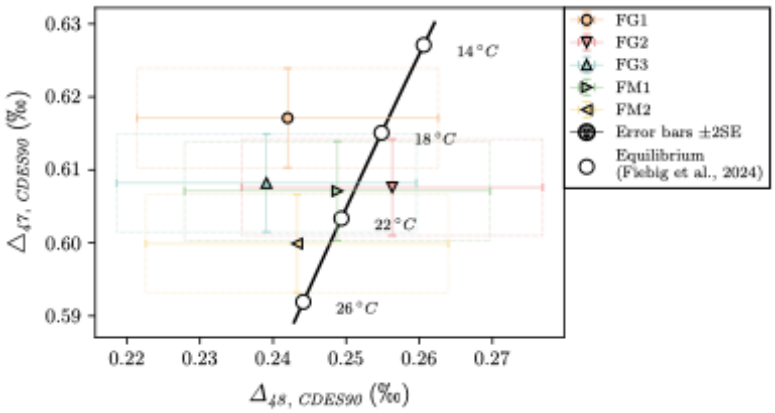

Fig. 2. Dual clumped isotope composition of Eocene molluscs.

Δ_{47}/Δ_{48} values of five Eocene samples are shown relative to the position of equilibrium (Fiebig et al., 2024). Modern molluscs are depicted in grey for comparison. Error bars indicate fully propagated 2SE.

Commented [DE27]: Same comments as on the previous figure

Commented [DE28]: This either needs to be deleted or the figure needs to be corrected

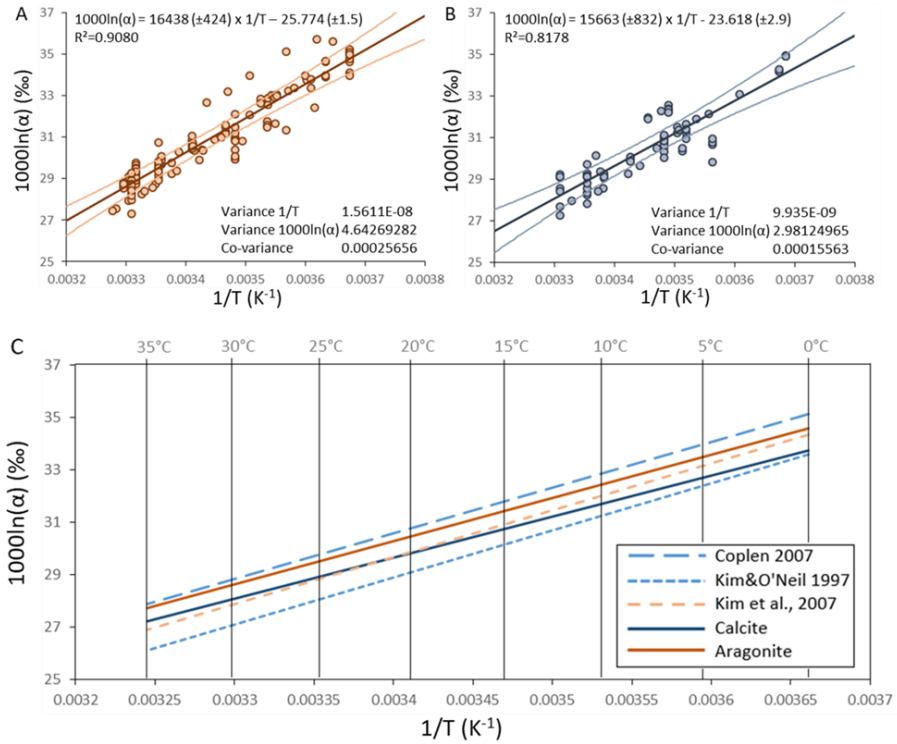

Fig. 3. Temperature dependence of the oxygen isotope fractionation between water and calcite and aragonite, respectively.

Compilation of empirical oxygen isotope fractionation data for aragonitic (A; in red; n = 154) and calcitic (B; in blue; n = 81) molluscs (Grossmann and Ku, 1986; Lecuyer et al., 2004; Lecuyer et al., 2012; Henkes et al., 2013; Caldarescu et al., 2021; de Winter et al., 2022; Huyghe et al., 2022; this study). Growth temperatures reflect measured water temperatures. For linear regressions (thick lines) in A and B, uncertainties in growth temperatures and 1000lnα were not considered as these were not consistently reported in each of these studies. Thin lines in A and B represent 95% confidence intervals of regression lines. A comparison of corresponding empirical regression lines with inorganic relationships obtained by Coplen (2007) and Kim & O'Neil (1997) for calcite, and Kim et al. (2007) for aragonite is shown in C.

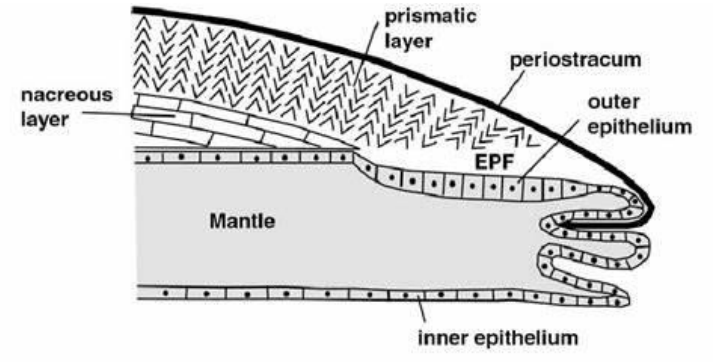

Fig. 4. Schematic drawing of the EPF (taken from Carré et al., 2006).

Shell formation in molluscs is orchestrated within the extrapallial fluid (EPF) which is enclosed by the outer epithelium (outermost cell layer of the mantle) and the periostracum (organic layer that covers the shell).

1196 **Table 1.** Metadata of the analysed molluscs samples.

Sample	Species	Origin	Sampled part	Mineralogy
RG1	*Buccinum undatum* LINNAEUS 1758	Fife, Scotland, UK	Whole shell	Ar
RG2	*Patella vulgata* LINNAEUS 1758	Fife, Scotland, UK	Whole shell	Cc (>80%) Ar
RG2_U	*Patella vulgata* LINNAEUS 1758	Fife, Scotland, UK	Subsample RG2, no oxidative cleaning	Cc (>80%) Ar
RM1	*Modiolus modiolus* (LINNAEUS 1758)	Fife, Scotland, UK	Whole shell	Ar
RM2	*Spisula solida* (LINNAEUS 1758)	Fife, Scotland, UK	Whole shell	Ar
AL_006	*Arctica islandica* (LINNAEUS 1767)	Grown in culture (NIOZ), NL	Bulk sample	Ar
CHA_M_050	*Arctica islandica* (LINNAEUS 1767)	Dredged from NE coast of Iceland	Bulk sample (dual clumped data in Staudigel et al., 2023)	Ar
CHA_M_062	*Arctica islandica* (LINNAEUS 1767)	Dredged from NE coast of Iceland	Bulk sample (dual clumped data in Staudigel et al., 2023)	Ar
M2-Sf	*Magallana gigas* (THUNBERG 1793)	Mokbaai, Texel, NL	Seasonally averaged, entire hinge, foliated microstructure Geochemical data in de Winter et al., 2021	Cc
M2Sv	*Magallana gigas* (THUNBERG 1793)	Mokbaai, Texel, NL	Seasonally averaged, 2nd growth year Geochemical data in de Winter et al., 2021	Cc
ME_002	*Mytilus edulis* LINNAEUS 1758	Grown in culture (NIOZ), Grevelingen, NL	Bulk sample, Respiration rate data in Jansen et al., 2007	Cc+Ar
ME_003	*Mytilus edulis* LINNAEUS 1758	Grown in culture (NIOZ), Grevelingen, NL	Bulk sample, Respiration rate data in Jansen et al., 2007	Cc+Ar
Shell UC	*Hippopus porcellanus* ROSEWATER 1982	Antique trade	Along growth lines (Nooitgedacht et al., 2021)	Ar
Shell UH	*Hippopus porcellanus* ROSEWATER 1982	Antique trade	Along growth lines (Nooitgedacht et al., 2021)	Ar
TS2	*Tridacna Squamosa* LAMARCK 1819	Aquarium, Royal Burgers' Zoo, Amden, NL	Part of the inner shell	Ar
WS2	*Hiatella arctica* (LINNAEUS 1767)	White Sea, RU	Avoiding areas of muscle attachment and hinge	Ar
WS3	*Tridonta borealis* (*Astarte borealis*) (SCHUMACHER 1817)	White Sea, RU	Avoiding areas of muscle attachment and hinge	Ar
FG1	*Sycostoma* sp. COX 1931	Barton on Sea, England, UK	Whole shell	Ar
FG2	*Turricula (Orthosurcula) rostrata* (SOLANDER 1766)	Barton on Sea, England, UK	Whole shell	Ar
FG3	*Strombus athleta* (SOLANDER 1766)	Barton on Sea, England, UK	Whole shell	Ar

FM1	*Bathytormus sulcata* (SOLANDER 1766)	Barton at Sea, England, UK	Whole shell	Ar
FM2	*Arcturellina pusilla* (DESHAYES 1858)	Barton at Sea, England, UK	Whole shell	Ar

*NIOZ: Koninklijk Nederlands Instituut voor Onderzoek der Zee

1198 **Table 2.** Independently constrained growth temperatures, Δ_{47}-derived growth temperatures and
1199 independently constrained $\delta^{18}O_{SW}$ of the investigated mollusc specimens.

Sample	**Growth temperature**	Δ_{47} **derived T (°C)**	**T-range 95% CI (°C)**	$\delta^{18}O_{SW}$ **(‰ vs VSMOW)**
RG1	MASST 9.6°C, Seasonal range 7-12.4°C	6.9	4.7-9.0	0.2 (Harwood et al., 2008)
RG2	MASST 9.6°C Seasonal range 7-12.4°C	9.1	7.5-10.7	0.2 (Harwood et al., 2008)
RM1	MASST 9.6°C Seasonal range 7-12.4°C	8.2	6.0-10.5	0.2 (Harwood et al., 2008)
RM2	MASST 9.6°C Seasonal range 7-12.4°C	8.2	5.9-10.5	0.2 (Harwood et al., 2008)
AL_006	Cultured at 12°C	12.3	10.0-14.6	-1.55
CHA_M_050	MASST 3.9°C Seasonal range 1.8-7.4°C	7.6	5.4-9.9	Approximate estimate ~0 (Schmidt et al., 1999)
CHA_M_062	MASST 3.9°C Seasonal range 1.8-7.4°C	5.1	2.9-7.4	Approximate estimate ~0 (Schmidt et al., 1999)
M2-Sf	MASST 11.5°C Seasonal range 4.5-19.2°C	19.0	16.9-21.1	-1.55
M2-Sv	MASST 11.5°C Seasonal range 4.5-19.2°C	12.1	10.2-14.0	-1.55
ME_002	Mean growth temperature 16.2°C Seasonal range 5-25°C	16.1	13.9-18.3	-1.55
ME_003	Mean growth temperature 16.2°C Seasonal range 5-25°C	15.4	13.1-17.7	-1.55
Shell UC	est. 27-31°C (based on geographic occurrence)	26.3	24.0-28.7	~0.1 (Schmidt et al., 1999)
Shell UH	est. 27-31°C (based on geographic occurrence)	28.3	26.1-30.5	~0.1 (Schmidt et al., 1999)
TS2	25.9°C, up to 26.8°C in summer	24.4	22.2-26.6	-1.05 (measured)
WS2	MASST 7.1°C Seasonal range 0.3-13.0°C	1.4	-0.4-3.2	-3.24
WS3	MASST 7.1°C Seasonal range 0.3-13.0°C	8.3	6.4-10.3	-3.24

1200

1201

1202

1203 **Table 3.** Stable and clumped isotope data of investigated molluscs. n represents number of analysed
1204 mollusc specimens.

Modern	$\delta^{18}O_{CO2}$ VSMOW [‰]	$\delta^{18}O_{CC}$ VSMOW [‰]	$\delta^{18}O_{CC}$ VPDB [‰]	$\delta^{13}C$ VPDB [‰]	Δ_{47} CDES90 [‰]	Δ_{47} 95% CI [‰]	Δ_{48} CDES90 [‰]	Δ_{48} 95% CI [‰]	**n**
RG1	41.31	32.50	1.53	1.12	0.6493	0.0068	0.2550	0.0210	9
RG2	40.99	32.60	1.63	0.93	0.6422	0.0050	0.2882	0.0159	21
RG2*	40.93	32.48	1.51	0.90	0.6441	0.0056	0.2904	0.0180	15
RG2_U	41.13	32.68	1.71	1.01	0.6377	0.0078	0.2836	0.0244	6
RM1	41.12	32.30	1.34	1.49	0.6450	0.0071	0.2545	0.0214	9
RM2	41.03	32.21	1.25	0.77	0.6451	0.0074	0.2500	0.0223	8
AL_006	41.79	32.97	1.99	0.05	0.6324	0.0070	0.2713	0.0225	7
CHA_M_050	42.76	33.96	2.95	1.29	0.6468	0.0071	0.2620	0.0231	7
CHA_M_062	43.19	34.36	3.34	2.30	0.6548	0.0072	0.2639	0.0232	7
M2-Sf	37.58	29.21	-1.66	-2.00	0.6122	0.0065	0.2644	0.0215	8
M2-Sv	37.72	29.35	-1.52	-1.84	0.6336	0.0062	0.2654	0.0204	9
ME_002	39.26	30.88	-0.04	-1.70	0.6209	0.0066	0.2535	0.0209	8
ME_003	39.19	30.81	-0.11	-1.41	0.6229	0.0070	0.2600	0.0221	7
Shell UC	37.99	29.20	-1.67	2.91	0.5909	0.0066	0.2425	0.0204	8
Shell UH	37.72	28.93	-1.93	2.44	0.5855	0.0062	0.2384	0.0194	9
TS2	36.69	27.91	-2.92	-7.42	0.5965	0.0064	0.2400	0.0214	8
WS2	41.21	32.39	1.43	1.64	0.6668	0.0059	0.2595	0.0187	10
WS3	37.30	28.52	-2.33	-0.05	0.6446	0.0061	0.2864	0.0195	9
Fossil									
FG1	36.61	27.83	-3.00	0.08	0.6171	0.0068	0.2420	0.0206	9
FG2	36.96	28.18	-2.66	-2.08	0.6076	0.0066	0.2563	0.0206	9
FG3	36.65	27.87	-2.96	-1.88	0.6082	0.0067	0.2391	0.0205	9
FM1	37.14	28.36	-2.48	1.20	0.6071	0.0068	0.2488	0.0209	9
FM2	35.73	26.96	-3.84	0.58	0.5999	0.0067	0.2433	0.0207	9

1205

1206 **Table 4.** Δ_{47}-derived temperatures and reconstructed seawater $\delta^{18}O$ for Eocene samples.

Sample	Δ_{47} **derived T (°C)**	**T-range 95% CI (°C)**	**Reconstructed $\delta^{18}O_{sw}$ (‰ vs VSMOW)**	**$\delta^{18}O_{SW}$-range 95% CI (‰ vs VSMOW)**
FG1	17.3	15.1-19.6	-3.5	-3.1 - -3.9
FG2	20.5	18.3-22.8	-2.6	-2.1 - -3.0
FG3	20.3	18.1-22.6	-2.9	-2.5 - -3.3
FM1	20.7	18.4-23.1	-2.3	-1.9 - -2.8
FM2	23.2	21.0-25.6	-3.2	-2.8 - -3.6

1207

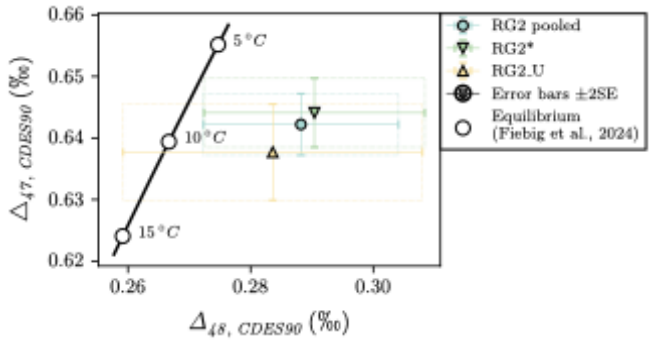

Supplementary Figure S1. Comparison of dual clumped isotope data obtained on bleached (*) and non-bleached aliquots (U) of RG2. Since the two samples are indistinguishable from each other within uneertainty (fully propagated 2SE), we pooled both aliquots.

Commented [DE29]: Same comment as figs1/2.

I may be wrong, please check, but I suspect GCA will either want this to be in an appendix or separated out into a supplementary materials file

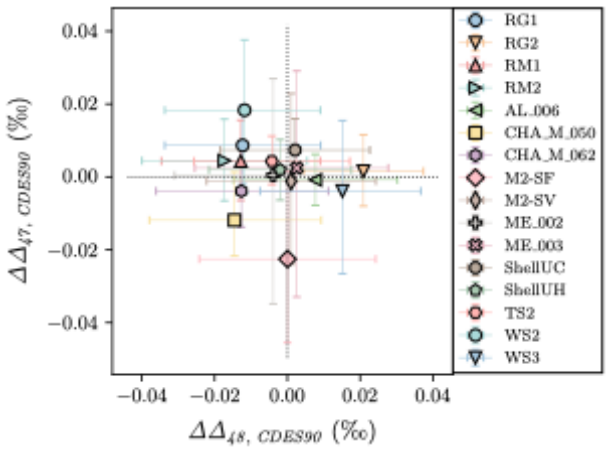

Supplementary Figure S2. Correlation plot of Δ_{47} disequilibrium vs Δ_{48} disequilibrium for the modern mollusc specimens. Error bars represent propagated uncertainties arising from habitat temperature uncertainty and analytical uncertainty. See Appendix A for further information.

Commented [DE30]: Where is this?

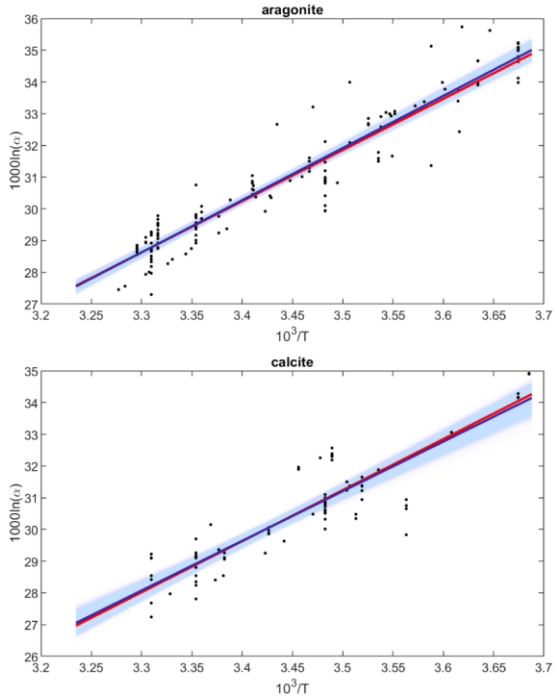

Supplementary Figure S3. Alternative (bootstrap) regression approach (cf. main text Fig. 3). Each of the datasets was resampled 10^4 times in order to understand the sensitivity of the ordinary least squares regression approach presented in the main text to possible outliers in the dataset. The bootstrap and OLS approaches are shown by the black and red lines, respectively, based on the 50th percentile of the 10^4 regression coefficients in the former case. The blue shaded region shows the 2.5th and 97.5th percentile range of the bootstrap coefficients.